AD-A133 170 RAPID MAGNETIC ENERGY RELEASE ITS POSSIBLE ROLE IN CORONAL HEATING AND SO..(U) SMITHSONIAN ASTROPHYSICAL OBSERVATORY CAMBRIDGE MA G L WITHBROE ET AL. 01 MAR 83 1/1

UNCLASSIFIED AFGL-TR-83-0086 F19628-82-K-0018 F/G 3/2 NL

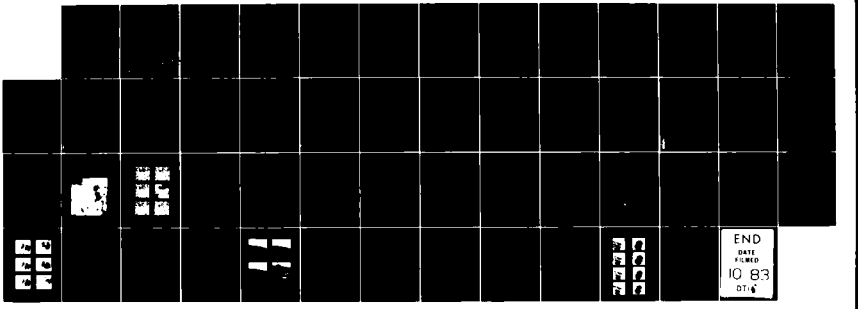

END
DATE FILMED
10 83
DTIC

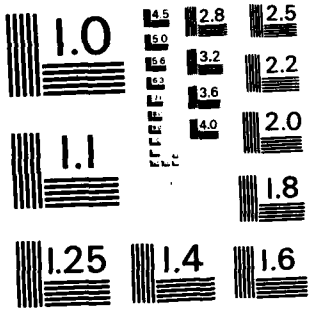

This report has been reviewed by the [illegible] Public Affairs Office [illegible] and is releasable to the National Technical Information Service (NTIS).

This technical report has been reviewed and is approved for publication.

S. L. Kell
Contract Manager

S. L. Kell
Branch Chief

FOR THE COMMANDER

[illegible]
[illegible] Director

[illegible]

[illegible]

[illegible]

Unclassified

SECURITY CLASSIFICATION OF THIS PAGE (When Data Entered)

REPORT DOCUMENTATION PAGE		READ INSTRUCTIONS BEFORE COMPLETING FORM
1. REPORT NUMBER AFGL-TR-83 - 0086	2. GOVT ACCESSION NO. A132170	3. RECIPIENT'S CATALOG NUMBER
4. TITLE (and Subtitle) RAPID MAGNETIC ENERGY RELEASE, ITS POSSIBLE ROLE IN CORONAL HEATING AND SOLAR WIND ACCELERATION		5. TYPE OF REPORT & PERIOD COVERED Final Report 1 Jan. 1982 - 31 Dec. 1982 6. PERFORMING ORG. REPORT NUMBER
7. AUTHOR(s) George L. Withbroe Shadia R. Habbal		8. CONTRACT OR GRANT NUMBER(s) F 19628-82-K-0018
9. PERFORMING ORGANIZATION NAME AND ADDRESS Smithsonian Institution Astrophysical Observatory 60 Garden Street Cambridge, MA 02138		10. PROGRAM ELEMENT, PROJECT, TASK AREA & WORK UNIT NUMBERS 61102F 2311G3CM
11. CONTROLLING OFFICE NAME AND ADDRESS Air Force Geophysics Laboratory Hanscom AFB, MA 01731 Monitor/Capt. S.L. Keil/PHS		12. REPORT DATE 1 March 1983 13. NUMBER OF PAGES 51
14. MONITORING AGENCY NAME & ADDRESS(if different from Controlling Office)		15. SECURITY CLASS. (of this report) Unclassified 15a. DECLASSIFICATION DOWNGRADING SCHEDULE

16. DISTRIBUTION STATEMENT (of this Report)

Approved for public release; distribution unlimited

17. DISTRIBUTION STATEMENT (of the abstract entered in Block 20, if different from Report)

18. SUPPLEMENTARY NOTES

19. KEY WORDS (Continue on reverse side if necessary and identify by block number)

Sun, Corona, Coronal Holes, Active Regions, Flares

20. ABSTRACT (Continue on reverse side if necessary and identify by block number)

Studies of the EUV emission from coronal bright points, active regions and spicules suggest that stochastic mechanisms may play an important role in heating the solar atmosphere at chromospheric and coronal levels. In small magnetic bipolar regions (spatial extent < 1') the observed EUV variations suggest that impulsive heating at chromospheric and coronal levels appears to be very important, possibly the dominant form of heating. The mechanism most likely involves rapid release of magnetic energy, possibly associated with the

DD FORM 1 JAN 73 1473 EDITION OF 1 NOV 65 IS OBSOLETE

Unclassified

SECURITY CLASSIFICATION OF THIS PAGE (When Data Entered)

(cont.)

emergence of magnetic flux from lower levels into the chromosphere and corona. In larger scale (> 1') magnetic bipolar regions, there is evidence for both quasi-steady and impulsive heating, with quasi-steady heating dominating. This heating could be caused by either a mechanism such as steady-state current dissipation, or by a stochastic process whose integrated effect (resulting from the smoothing caused by finite radiative and conductive cooling times) yields a nearly constant radiative output. The widespread variability of the emission in spectral lines formed at transition region temperatures ($10^5 < T < 10^6$ K) provides evidence that impulsive energy releases are a common, nearly continuous phenomenon in bipolar magnetic regions. However, at the present time we do not know what fraction of the total energy deposition in the atmosphere (chromosphere and low corona) originates in impulsive phenomena.

TABLE OF CONTENTS

1. INTRODUCTION

One of the fundamental problems of solar physics is determination of the coronal heating mechanism. For many years, it was widely believed that upward propagating acoustic waves were the primary means by which energy was transferred from the solar convection zone to the corona. However, observations from OSO-8 (cf. Athay and White 1978a, 1978b) indicated that acoustic waves deliver insufficient energy to the corona to balance the observed radiative and convective energy losses. This finding, coupled with the observation that spatial variations in coronal heating appear to be intimately linked to the strength and configuration of the coronal magnetic field, has led to renewed interest in heating mechanisms based on the dissipation of energy stored in magnetic fields (see reviews by Withbroe and Noyes 1977, Valana and Rosner 1978, Wentzel 1981). There are a variety of possible mechanisms for releasing this energy. Some yield quasi-steady state heating (e.g. heating by steady currents), while others involve transient, impulsive heating (e.g. rapid reconnection). A solar flare is an example of a sudden, impulsive energy release resulting in plasma heating. The objective of the present study was to look for observational signatures of coronal heating processes, particularly signatures provided by temporal and spatial variations of the EUV emission from regions with strong magnetic fields.

The study was motivated by the results of an earlier investigation by Habbal and Withbroe (1981) who found that a number (9) of coronal bright points located in an equatorial coronal hole exhibited large variations in EUV emission on time scales of minutes. Coronal bright points are small (10"-30") areas of enhanced coronal emission overlying regions where the photospheric magnetic field is bipolar. The intensity variations found by Habbal and Withbroe took place within substructures of the bright points, which most likely consist of miniature magnetic loops that evolve on time scales of a few minutes. The EUV observations suggest that the plasma in coronal bright points is heated by an intermittent, impulsive heating mechanism, most likely involving the rapid release of magnetic energy.

These results raise questions concerning the role of impulsive heating as a general mechanism for coronal heating. Are all coronal regions heated primarily by an impulsive mechanism, or only small scale rapidly evolving features such as the bright points studied by Habbal and Withbroe? What happens in other types of regions? The study by Habbal and Withbroe was confined to a relatively small number of bright points in a limited area of the disk in a large equatorial coronal hole. As we show below, impulsive heating appears to occur in coronal loops ranging in size from 5"-30" in coronal bright points to several arc minutes in active regions. However, in many cases, particularly for the larger scale loops, the impulsive heating appears as an "ac" signal superimposed on a "dc" signal of larger amplitude (by a factor of 10 to 20) except for occasional flare-like enhancements.

2. IMPULSIVE PHENOMENA IN CORONAL BRIGHT POINTS

The EUV observations used in the present investigation were acquired by the Harvard Skylab Experiment (cf. Reeves et al. 1978a, 1978b). Most of the data consist of 5' x 5' spectroheliograms in selected spectral lines between 300 and 1350 Angstroms. The spatial resolution was 5". Figure 1 contains a spectroheliogram in Mg X λ625 acquired in an equatorial coronal hole. The large dark area crossing the spectroheliogram from the lower left to the upper right is the coronal hole. The nine bright points studied by Habbal and Withbroe (1981) are circled. Figure 2 contains a set of spectroheliograms showing the appearance of a bright point (circled) at chromospheric (Ly α), transition region (C II, C III, O IV and O VI) and coronal (Mg X) temperatures. The larger bright patch of emission below the bright point is a small active region which we studied during the course of the present investigation (see Section 3). Sets of spectroheliograms such as these were obtained at 5.5 minute intervals by the Harvard instrument in its normal operating mode. The instrument could monitor up to seven wavelengths simultaneously with its photoelectric detection system. Most of the data were acquired in the six wavelengths given in Figure 2, however, occasionally other combinations were used, particularly one yielding simultaneous observations in Ne VII λ465 and Si XII λ521.

The primary cooling mechanisms for the coronal plasma in a closed magnetic loop appear to be radiation and electron thermal conduction. (The latter transports energy from the corona to the transition region and upper chromosphere where the energy is lost from the atmosphere by radiation). Habbal and Withbroe (1981) determined that the cooling time due to the combined effect of these two loss mechanisms was 100 to 300 seconds. Hence, if the coronal plasma in a bright point is heated by an impulsive heating mechanism with the time between impulses greater than or equal to 100 to 300 seconds, one would expect to observe variable coronal emission from these features. (See Rosner et al. 1978, and a review by Withbroe 1981 for a discussion of the relationship between coronal energy deposition and coronal emission.) The emissions from the transition region and the upper chromosphere are sensitive to the downward conductive flux, which depends critically on the coronal temperature; thus, the emission from these layers can also be affected by variable energy inputs to the corona. Habbal and Withbroe found that the emissions at all three levels (chromosphere, transition region, and corona) varied on a time scale of a few minutes and that these variations were generally correlated.

One can also obtain variable emission at chromospheric, transition region, and possible coronal levels if the energy release is in the chromosphere (or transition region). In the latter case, the coronal emission will vary only if significant amount of coronal material is heated to coronal temperatures (or if the energy deposition leads to a compression of coronal material). We discuss this point further in later sections.

An example of the type of intensity variations found by Habbal and Withbroe for a coronal emission line (Mg X λ625) is shown in Figure 3. These variations are from a small equatorial bright point (No. 3 in Fig-

ure 1). For the present investigation we selected a series of 8 bright points in a polar coronal hole. These bright points tended to be several times larger than those studied by Habbal and Withbroe and generally showed less dramatic intensity variations. Figure 4 illustrates a typical set of data for Mg X λ625. The total intensity in a 25" x 30" area was determined by summing the intensities in the 54 pixels in the selected area (designated BP-A), where the intensity is measured in counts per integration time (0.040 sec) of the photoelectric detection system of the experiment. The upper graph in Figure 4 gives the total intensity as a function of time. The temporal spacing between the points is 5.5 min. The peak-to-peak fluctuations are approximately 20% of the mean intensity. Since we were interested primarily in detection of intensity variations, most of the remaining graphs in this report are similar to the lower graph in Figure 4 which gives only the time-varying part of the intensity. The short vertical lines passing through the individual data points are the expected range ($\pm$ 1 σ) of the intensity due to counting statistics ($\sigma = \sqrt{N}$ where $\overline{N}$ is the number of counts). Using plots of this type one can easily establish whether or not there are significant temporal variations in the emission from a given region.

As in the Habbal and Withbroe study, we found that the variations in the emissions from the coronal bright points comes from substructures in the regions, where at a given time the intensity variations occurred primarily in a few pixels out of the 30 to 60 typically defining a bright point. If the intensity fluctuations in these few pixels are not large, they may cause only insignificant variations in the total emission from the region. This is illustrated for BP-A in Figure 5. The upper graph shows the variation in the emission (in O VI λ1032) from the entire bright point which covers an area of 25" x 40", while the lower graph shows the temporal variation of the emission from a 10" x 15" area that exhibited significant fluctuations. (By significant variations we mean variations whose magnitude is substantially larger than that expected due to statistical fluctuations in the signal measured by the instrument.)

Seven other polar bright points were studied. Often there was a good correlation between intensity fluctuations observed at chromospheric (Ly α λ1216, $T \simeq 2 \times 10^4$ K), transition region (e.g. O VI λ1032, $T \simeq 3 \times 10^5$ K) and coronal (Mg X λ625, $T \simeq 1.5 \times 10^6$ K) temperatures. As illustrated in Figures 6 (BP-B), 7 (BP-C) and 8 (BP-D), where, for example, the largest enhancements in the transition region line (O VI λ1032) correspond to similar enhancements at coronal (Mg X λ625) and chromospheric (Ly α λ1216) temperatures. However, there are also cases where significant fluctuations at one level are not accompanied by corresponding fluctuations at other levels, as shown in Figure 9 (BP-E).

The lack of correlation appears to be due to several factors. Studies of surges in active regions (see Section 7), EUV emission from spicules (see Section 6), and macrospicules (Withbroe et al. 1976) indicate that the deposition of energy at chromospheric levels can result in the ejection of cool ($T < 10^6$ K) material that produces enhanced emission at chromospheric and transition region temperatures, but not at coronal temperatures. That is, the ejected material appears to remain at temperatures less than 10^6 K (or if it is heated to higher tempera-

tures, the plasma heating occurs in such a fashion that enhancements in coronal emission are not observed). At chromospheric and/or transition region temperatures these ejecta often are brighter than the surrounding regions, thereby producing a local enhancement in the appropriate spectral lines. In some cases, EUV brightenings observed at chromospheric and/or transition region temperatures were associated with nearly simultaneous "flare-like" enhancements at adjacent pixels. (By flare-like we mean rapid intensity increases observed simultaneously at chromospheric through coronal levels). We believe that these chromospheric/transition region brightenings are produced by small surge-like mass ejections.

Another possible cause of the lack of correlation between emissions from various heights is that when energy is released in a given layer there is insufficient energy transport to a higher and/or lower layers to alter significantly the emissions from those layers. For example, in some cases radiative cooling may dominate over conductive cooling leading to minimal energy transport to adjacent regions by thermal conduction. A third factor is that the large opacity in the optically thick chromospheric lines (e.g. Ly α) may mask (or through opacity changes, perhaps cause) variations in the chromospheric emission.

3. IMPULSIVE PHENOMENA IN A SMALL ACTIVE REGION

In order to investigate the occurrence of impulsive phenomena in regions with larger spatial scales than coronal bright points, we analyzed EUV measurements of the small active region shown in Figures 1 and 2 (the largest patch of bright emission in the upper right-hand quadrant). This region exhibited nearly continuous "flare-like" enhancements. This is shown in Figures 10-13. Figures 10-12 show the spatial variations in Mg X λ625, while Figure 13 shows the variations in the integrated EUV emissions from chromospheric (Lyman α), transition region (C III, O IV and O VI) and coronal lines. The left-hand plots in Figure 13 are for the eastern patch of emission in the active region (see Figures 10-12, also brightest patch in upper right-hand quadrant of Figures 1 and 2), while the right-hand plots are for the emissions from the western part of the region (right-hand patch of emission in Figures 10-12). As was the case for the coronal bright points studied by Habbal and Withbroe, the EUV brightenings occurred at a variety of different locations in the active region and occasionally spilled over into adjacent quiet regions. In Figure 13 the intensity peaks at 0524 and 0603 in the left-hand plots correspond to the subflares whose spatial extent and locations are shown in Figure 10. Note now the southern (lowest) portion of the region brightens first on the right (0603) and then left (0609). The Mg X λ625 emission in this area of the active region is particularly variable as is apparent from a careful examination of Figures 10-12.

In Figures 10 through 12 one can observe the growth of the western area of the active region (area of enhanced emission on right-hand side of the figures). This area gradually merges with the left-hand or eastern region via a connecting "bridge" of coronal loops that forms between the two regions (see Figure 12 where the bridge is sufficiently bright in MgX to be prominent in the contour maps). One may speculate that the two regions and their connecting "bridge" were formed by mag-

netic flux emerging from lower levels of the atmosphere and that the intensity variations and "flare-like" brightenings were caused by the rapid release of energy stored in the magnetic fields. Due to the youth of the regions the energy storage (via stressing of the field lines) most likely occurred prior to emergence into the corona. The release of stored energy could have been triggered after the field lines emerged and the magnetic forces became larger than those exerted by the plasma when the field lines moved upward into the less dense regions of the atmosphere. (In the photosphere and below the gas pressure is larger than the magnetic pressure.) Alternatively, the energy release could have been triggered when newly emerging flux tubes interact with those that had emerged earlier, a scenario similar to that which has been suggested to occur in some flares in active regions.

The variations of the integrated EUV intensities from the western area of the active region are shown in Figure 13. Note the numerous short term brightenings and longer term enhancement starting at about 0700 UT. The latter began declining at about 0840 UT in the cooler ($T < 10^6$ K) lines (note in particular O VI) shortly after the loops connecting the eastern and western areas became sufficiently bright to be prominent in Mg X (see Figure 12). Also note that the mean brightness of the eastern region (Figure 13) decreases, particularly in transition region lines, prior to the enhancement in the western region at approximately 0700.

Given the spatial and temporal variations in the EUV emission in the small active region (denoting the coalesced region in Figures 10-12 as a small active region), it appears that the coronal heating in this area is dominated by heating processes with a stochastic nature. These heating processes most likely involve rapid release of magnetic energy.

4. STOCHASTIC HEATING IN SMALL BIPOLAR MAGNETIC REGIONS

The EUV observations of the small active region discussed above coupled with the results of the analysis of EUV observations of 17 coronal bright points (9 by Habbal and Withbroe, and 8 in the present study), suggest that stochastic processes play an important, perhaps dominant, role in the heating of the upper chromospheric, transition region and coronal plasmas in small scale magnetic bipolar regions. The following hypothesis is suggested. It is a scenario similar to that which has been suggested for flares in active regions (cf. Sturrock 1980). Magnetic flux tubes emerge from the lower atmosphere. The energy stored in these tubes (e.g. via twisting of the field lines into non-potential configurations) is released suddenly resulting in plasma heating, most likely at coronal levels. Energy is transferred to the chromospheric footpoints of the magnetic loops via thermal conduction and/or accelerated particles. This deposition of energy into the chromosphere heats up the upper chromospheric material which flows upward filling the loop with hot, dense plasma via "chromospheric evaporation". There is a "burst" of EUV emission lasting from several minutes due to the plasma heating, when the plasma cools and drains from the loop. The enhanced EUV emission is produced at chromospheric, transition region and coronal levels. Some energy release may occur in the chromosphere and/or transition region producing surge-like phenomena or small mass

ejections that produce enhancements in chromospheric and/or transition region emissions without corresponding enhancements of the coronal emission at the same location.

5. STOCHASTIC PLASMA HEATING IN ACTIVE REGIONS

As discussed above, EUV observations suggest that stochastic processes play an important, if not dominant role in plasma heating for coronal loops found in small magnetic bipolar regions, such as coronal bright points and small active regions. In order to see if this may also be the case for larger loops, we analyzed Skylab EUV observations of two active regions.

Figure 14 contains a series of spectroheliograms showing the two regions which were located near the east limb at the time the observations were acquired. The spatial and temporal variations in the loop structures observed in the region closest to the limb (McMath region 12634) indicate that the plasma in the highest lying loops is apparently thermally unstable. The emission in spectral lines formed at temperatures below 10^6 K, especially O VI λ1032 and Ne VII λ465, exhibited large spatial and temporal variations. In addition, the emission from these lines was observed at heights far above that expected for plasma that is in hydrostatic equilibrium. The data suggest that these emissions were produced by coronal plasma that was cooling by radiation, became thermally and dynamically unstable (that is, developed a Raleigh-Taylor instability) and flowed downward along the magnetic field lines to the chromosphere. We also found that the emission originating near the surface at transition region temperatures ($10^5 < T < 10^6$ K) was variable throughout both active regions shown in Figure 14. An example of this variability is shown in Figure 15 (lower graphs) for the O VI emission from the footpoints of the loops in the McMath region 12634.

The emission from the "coronal" lines ($T > 10^6$ K) Mg X and Si XII generally was much more constant and exhibited smaller (< 10%) fluctuations in intensity. This is illustrated for the emission near the loop footpoints (Figure 15) and several positions in the loops at heights greater than 10^4 km above the surface in McMath region 12634 (see Figure 16). One does find occasional small-scale impulsive enhancements in the "coronal" lines such as those occurring at 7.5 hours in Figure 15 and at 7.42 hours in Figure 16. Larger subflare-like enhancements in intensity are also observed, as illustrated in Figure 17 which shows two impulsive enhancements that occurred near the loop footpoints An McMath region 12628 (the foreground region in Figure 14).

The observations of McMath regions 12628 and 12634 indicate that quasi-steady heating appears to dominate in larger scale (>1') magnetic loops. This is in contrast to the small scale (<1') loops found in coronal bright points for which impulsive heating appears to be much more important. The evidence for quasi-steady heating in large active region loops is provided by the "dc" component of the coronal emission, which shows little variation on time scales of approximately an hour. One possible heating mechanism is the steady-state current dissipation (cf. Tucker 1973, Wentzel 1981). An alternative possiblity is that the heating mechanism is impulsive, but that the frequency of the energy

releases and/or summation along the line of sight produces quasi-steady heating (on the time scale of the radiative and conductive cooling rates) and the resulting nearly constant radiative output observed in the EUV. Some evidence that impulsive energy releases are frequent is provided by the variability of the emission in spectral lines formed at transition region temperatures ($10^5 < T < 10^6$ K). In these lines the amplitude of the "ac" signal is substantially larger (approximately 10 to 50% relative to the dc level) than in the higher temperature lines. The "ac" component of the EUV emission in the hotter lines such as Mg X, which typically appears to have an amplitude of a few percent of the "dc" signal, indicates that impulsive energy releases do occur at coronal levels, however, the amount of energy involved in these detectable impulsive events is a small fraction (few percent) of that producing the quasi-steady heating.

6. STOCHASTIC ENERGY RELEASE IN THE QUIET CHROMOSPHERE

There is one well known phenomena that is clearly associated with the stochastic release of energy at chromospheric heights, spicules. Spicules are jets of chromospheric material that are driven by an unknown mechanism to heights up to 15,000 km above the surface. Driving mechanisms that involve rapid release of magnetic energy and/or upward propagating MHD waves have been suggested (see Beckers 1968, 1972, Hollweg et al. 1982, Shibata 1982).

Very little is known about the role of spicules in the transport of mass and energy between the chromosphere and higher layers of the atmosphere. Recently Athay and Holzer (1982) suggested that the rise and fall of spicular material can supply the thermal energy required for heating the upper chromosphere, transition region and possibly corona. The mechanism is based on the inference that spicular material is raised well above the height that would be achieved by a projectile moving with the velocity typically observed for spicules (20 to 25 km s^{-1}). The gravitational potential energy gained during the spicular rise may then be converted into flow energy as spicular material falls and into internal energy as the fall is slowed, thus providing a source of heat for the atmosphere. The proposed mechanism depends upon assumptions about the fate of spicules after they disappear from view in the visual spectrum where observations are limited to spectral lines formed at chromospheric temperatures. In order to obtain information about the behavior of higher temperature material associated with spicules, it is necessary to make use of observations at wavelengths shortward of 2000 Angstrom, particularly the extreme ultraviolet (EUV), $300 < \lambda < 1400$ Angstrom where there are many strong resonance lines formed at temperatures between 2×10^4 and 2×10^6K. Although the spatial resolution of existing EUV data is inadequate to resolve individual spicules, EUV observations acquired by the Harvard Skylab experiment have sufficiently high resolution (5") to place limits on the heights of EUV emitting spicules and their effects on the overlying corona. The present report describes results of an analysis of measurements of the spatial and temporal variations of EUV emission near the solar limb. These results place empirical constraints on the fate of spicules after they disappear from view in the visible spectrum and thereby place contraints on their role in

the transport of mass and energy betweeen the chromosphere and corona.

As observed in the visible region of the spectrum, spicules cover about 1% of the solar surface, originate in the chromospheric network and rise to a maximum height of about 15,000 km above the photosphere (Beckers 1968, 1972; Athay 1976). One of the fundamental questions to be answered is how high spicules rise before they either fall back or are heated to coronal temperatures (and thereby cease to be spicules). A primary objective of the study reported in this section was to answer the above question.

Figure 18 contains several spectroheliograms acquired in a quiet region near the limb. These spectroheliograms were acquired simultaneously in all spectral lines. The jagged appearance of the limb is due to EUV emitting inhomogeneities extending beyond the limb. In the remainder of this paper we will refer to these inhomogeneities as spicules, although it is possible that they may also be due to clumps of cool ($T < 10^6$K) material resulting from the downflow of coronal material that has cooled and is falling into the chromosphere. The reason for attributing the inhomogeneities to spicules is their similarity in appearance (for example in hydrogen Lyman-α) to spicules observed with higher spatial resolution in Hα. As we shall see below, the scale height of these inhomogeneities is the same as that measured for Hα spicules.

One method of obtaining information about the height distribution of the inhomogeneities (which we are associating with spicules) is through use of measurements of the variation of the mean intensity with distance ρ (in units of a solar radius R_{sun}) from sun-center. Figure 19 gives $I(\rho)$ for CIII λ977 determined from measurements (points) in a typical quiet region of the limb. The emission beyond the limb ($\rho > 1$) decreases rapidly with increasing ρ, falling by nearly 3 orders of magnitude by $\rho = 1.03$. The emission scale height is approximately 1900 km. The relatively shallow gradient in the intensity fall off beyond $\rho = 1.03$ is most likely due to instrumentally scattered light from the disk (see Withbroe 1983a).

Measured EUV emission scale heights can be used to estimate the scale height H_s of EUV emitting spicules. We made use of a model developed by Withbroe and Mariska (1976). The model consists of a spherically symmetric, geometrically thin transition region through which cylindrical spicules extend. The spicules are assumed to be oriented radially, distributed randomly across the solar surface and to have a number density N_o identical to that determined for spicules observed in the visible (cf. Beckers 1968, 1972). The number of spicules extending to height h is assumed to be

$$N_s(h) = N_o e^{-h/H_s}. \qquad (1)$$

For the zero height we used the value 2000 km above the photosphere (optical depth unity at 5000 Angstrom). This appears to be approximately the height where the "homogeneous" chromosphere terminates and from which spicules originate (cf. Beckers 1968, Vernazza, Avrett and Loeser

1981).

Scale heights were derived using data acquired in three areas at the limb. Two of the areas were located near the south solar pole and the other in the quiet region shown in Figure 18. One of the polar areas was located in a coronal hole and the other in an adjacent quiet region. Values for H_s determined from measurements of several spectral lines and the H I Lyman continuum are given in Table 1. Figure 19 compares calculated intensities for C III λ977 with those measured in a quiet region. The calculated intensities were smoothed with the instrumental slit function for comparison with the observations. In order to demonstrate the sensitivity of the calculated intensities to variations in the assumed spicular scale height, curves are given for H_s = 0, 1900 and 2500 km. Figure 20 compares calculated intensities for several wavelengths with measurements from the south polar coronal hole. The differences in the amount of limb brightening for $\rho < 1$ for the various wavelengths are due to differences in the optical depths (at these wavelengths) of spicules and the transition region (see Withbroe and Mariska 1976). The derived spicular scale heights depend primarily on the gradients $dI(\rho)/d\rho$ for $\rho > 1$ and are insensitive to model parameters controlling amount of limb brightening on the disk. Also shown in Figure 20 are intensities from higher temperature lines to be discussed later. The mean temperature of formation for each line is given in Table 1 (cf. Dupree 1972).

The mean scale height for the EUV emitting inhomogenities, 2000 km ± 300 km, is in good agreement with that obtained for Hα spicules, 1750 km (see review by Beckers 1972). In an earlier paper we demonstrated that EUV limb intensities calculated with a scale height of 1750 km gave a good fit to EUV limb intensities measured for several quiet regions within 40° of the equator (Withbroe and Mariska 1976). Although exceptionally large spicules, known as macrospicules (Bohlin et al. 1975, Withbroe et al. 1976) which extend several times farther above the limb than ordinary spicules, are observed in EUV observations of polar coronal holes, they contribute only a small fraction of the total EUV emission measured at the limb and apparently do not significantly increase (< 10%) the mean scale height of EUV emitting spicules of coronal holes.

These data indicate that the bulk of the EUV emission in spectral lines formed at $T < 2 \times 10^5$ K originates at heights below 15,000 km. Through use of information in the measured limb brightening curves one can easily show that 99% or more of the emission in the lines formed at $T < 3 \times 10^6$ K originates at heights below 15,000 km ($\rho < 1.02$), which is equal to the average maximum height of Hα spicules. These results indicate that spicules not only fade from view at heights beyond 15,000 km when observed in visible lines such as hydrogen H-α, they also do so when observed in lines formed at much higher temperatures, $2 \times 10^4 K < T < 2 \times 10^5 K$.

One can also analyze the vertical extent of small scale spatial EUV inhomogenities to obtain constraints on spicule scale heights. We found that these inhomogeneities disappear into the noise at heights above 15,000 to 20,000 km above the limb, as might be expected from the emission gradients discussed above. More details on this phase of the

analysis are given by Withbroe (1983a).

A third method for obtaining information on the heights of EUV emitting spicules is through measurements of temporal variations in EUV intensities. On December 10, 1973, Astronaut Dr. E. Gibson acquired a series of spectroheliograms in the south polar coronal hole with a temporal resolution of about 1.7 minutes over a period of 40 minutes. Each spectroheliogram consists of a series of 5" x 5' scans parallel to the limb. For each of the 120 pixels (5" x 5" pixels measured at intervals of 2.5") in a scan, the magnitude $\sigma_t(i)$ of the RMS temporal fluctuations in intensity is defined by

$$\sigma_t(i)^2 = \sum [I_i(t) - \bar{I}_i]^2/n \qquad (2)$$

where $I_i(t)$ is the intensity of pixel i measured at time t, $\bar{I}$ is the mean intensity, n is the number of pixels summed and the summation is over time. Figure 21 shows $\sigma_t(i)/\sigma_e(i)$ (where $\sigma_e(i) = \bar{I}_i^{1/2}$) for a series of scans in C III λ977 made at different positions as measured by ρ, where ρ is the mean distance of the scan line from sun-center. Due to the curvature of the limb the pixels at either end of the scans are approximately 8000 km higher above the limb than the pixels near the center of the scan. We see that the RMS temporal fluctuations measured by $\sigma_t(i)/\sigma_e(i)$ disappear ($\sigma_t/\sigma_e \simeq 1$) at most pixels for heights $\rho \geq 1.03$ ($h \simeq 20{,}000$ km) except for a few pixels. Macrospicules, exceptionally large spicules found in polar coronal holes, cause the fluctuations at these latter pixels (cf. Withbroe et al. 1976).

Figure 22 compares the temporal fluctuations measured at the limb for $\rho \simeq 1.005$ ($h \simeq 3500$ km) for a series of spectral lines. The plots are arranged in ascending temperature of formation from the chromospheric line Lyman-α, the transition region lines of C III, O IV, O VI to the Mg X coronal line. There is a good correlation between the locations which have large temporal fluctuations in the chromospheric and transition region lines. The magnitude of the temporal fluctuations increases with increasing temperature, reaching a maximum at C III and then declining, essentially disappearing in Mg X λ625. This effect is illustrated as a function of distance from sun center in Figure 23 where we have plotted the parameter $\sigma_t(\rho)/\sigma_e(\rho)$ as a function of ρ where $\sigma_t(\rho)/\sigma_e(\rho)$ is the mean value of the RMS temporal fluctuations measured at a distance ρ from sun center. In the cooler lines, (Lyman-α, C III) the temporal fluctuations peak between $\rho = 1$ and 1.02. A similar peak is found in the O IV and O VI lines, along with a peak of comparable magnitude on the disk ($\rho < 1$), while the coronal Mg X line shows very little variation (in time) over the range of distances covered. These data further reinforce the conclusion drawn above that EUV emitting spicules disappear at heights approximately 15,000 to 20,000 km above the limb ($\rho \simeq 1.025$). The small temporal variations observed above that height are due to several macrospicules (see Figure 21 and Withbroe et al. 1976).

One can also use the EUV measurements to place limits on the mass M of cool material at large heights ($h > 17{,}000$ km) above the surface. This information can then be used to determine whether or not the energy

released by gravitationally accelerated downward falling cool material is a significant factor in the global energy balance of the atmosphere. The value found for M is 2-3 x 10^{-7} g cm^{-2}. The gravitational potential energy of this material is of the order 3-9 x 10^{7} erg. The maximum rate at which this energy E_p can be released is E_p/τ_{ff}, where τ_{ff} is the free-fall time. This yields a maximum globally averaged heating rate of 10^{5} erg cm^{-2} s^{-1}. For comparison the requirement for heating the upper chromosphere is approximately 3 x 10^{5} erg cm^{-2} s^{-1}. The coronal heating requirement is of the same order of magnitude (see review by Withbroe and Noyes 1977). Given that E_p is an upper limit and that E_p/τ_{ff} is the maximum energy release rate, these results suggest that release of gravitational potential energy of cool material is not the primary source of heating for the upper chromosphere, although it may make a non-negligible contribution. The maximum downward particle flux $n_p v$ associated with this material, 2 x 10^{14} cm^{-2} s^{-1}, is nearly an order of magnitude smaller than the downward particle flux in the transition region ($\simeq$ 10^{15} cm^{-2} s^{-1}) as deduced from UV observations (see Athay and Holzer 1982). Hence, infalling cool material from heights h $\geq$ 17,000 km is not the primary source of the mass in the downflows observed in the transition region.

To summarize: Three separate types of observational evidence derived from EUV measurements, (1) gradients in EUV emissions for p > 1, (2) spatial inhomogeneities and (3) temporal inhomogeneities as measured by σ_t, all indicate that EUV emitting spicules disappear at heights h $\simeq$ 15,000 km km essentially the same height at which Hα spicules disappear. The close agreement between the scale heights H_s of Hα spicules and those derived here for EUV emitting inhomogeneities observed near the limb is consistent with the assumption that the latter inhomogeneities are associated with Hα spicules. One likely possibility is that the EUV emission originates in a thin transition sheath separating the cool Hα emitting spicular material from the hotter surrounding corona.

One can now ask what role spicular material plays in atmospheric heating. As indicated earlier, Athay and Holzer (1982) have suggested that the release of gravitational potential energy by downward flowing spicular material may be an important source of atmospheric heating. For this to be the case for chromospheric material that is accelerated upward without being heated to high temperatures (T > 5 x 10^{5}K) the material must be raised to heights much larger (by a factor of 3) than those determined above. The energy required to raise chromospheric material to the heights observed for Hα and EUV emitting spicules is on the average a few times 10^{24} erg per spicule. If this energy is converted into thermal energy when the spicular material falls back into the chromosphere, the amount of energy released at the base of the spicule is about 10^{6} erg cm^{-2} s^{-1}. Since this is comparable to the amount of energy radiated in the upper chromosphere at the base of spicules, falling spicular material may provide a significant fraction of the energy required to heat these areas. However, falling cool spicular material most likely represents only a small fraction (a few times 10^{4} erg cm^{-2} s^{-1} or ~10%) of the globally averaged heating in the upper chromosphere (cf. Withbroe and Noyes 1977).

Significant amounts of spicular material may also be heated to

coronal temperatures as proposed by Pneuman and Kopp (1978) and others. Observations of the spatial and temporal variations of the emission from these features place limits on the conditions under which large amounts of spicular material can be heated to coronal temperatures. The EUV observations indicate that most of this heating, if present, occurs at heights h<15,000km. An additional observational constraint on the heating is that the heating rate must be sufficiently slow that the spicular material expands in approximate pressure equilibrium with the corona. This is required in order to avoid significant temporal or spatial fluctuations in the Mg X emission at the limb. On the other hand, the heating must be sufficiently rapid that the cool spicular material "disappears" from view within the lifetime of spicules, which typically is of the order of 5 min for spicules observed above the limb in Hα. The temporal sequence of EUV observations in the polar coronal hole discussed above yields similar lifetimes for EUV emitting spicules. The energy required to heat all of the cool ($T \simeq 1.6 \times 10^4$ K) material in a spicule to coronal temperatures ($T \simeq 1.5 \times 10^6$ K) is of the order of 10^{26} erg. This is 2 orders of magnitude more energy than required to lift cool chromospheric material to the observed heights. Thus, if spicular material plays a significant role in the chromospheric-coronal energy balance, it most likely does so by being heated to coronal temperatures at low heights ($h \leq 15{,}000$ km).

It should be noted that there is no direct observational evidence that significant amounts of spicular material are heated to coronal temperatures. This hypothesis has been advanced to account for the systematic red shifts observed in UV lines formed at temperatures $T \simeq 10^5$ K and the finding that the mass flux associated with the red-shifted material is comparable to the upward mass flux associated with cool ($T \simeq 1.5 \times 10^4$ K) spicular material (Pneuman and Kopp 1978). Under this hypothesis the emission measure of the upward moving material which is being heated must be much lower than that of the downward moving material which is cooling from coronal temperatures and falling into the chromosphere. The UV observations can be equally well explained by having spicular material heated to temperatures of 1 to 2 $\times 10^5$ K and then falling back into the chromosphere. This would also explain the finding reported here that the largest spatial and temporal fluctuations are observed in the intensities of EUV lines formed at these temperatures. It is interesting to note that the radiative loss function for a fully ionized plasma has a maximum at these same temperatures (Cox and Tucker 1969, Raymond, Cox and Smith 1976). The amount of energy required to heat spicular material to these temperatures is an order of magnitude smaller than if the material is heated to coronal temperatures.

It also must be pointed out that existing observations, including those presented here, do not rule out the possibility that large amounts of spicular material are heated to coronal temperatures. However, the present analysis indicates that this heating, if present, must occur primarily at heights below 15,000 km and must not cause large fluctuations in the emission of coronal lines formed at temperatures near 1.5 $\times 10^6$ K, the mean temperature of formation of the Mg X line. In order to establish how much spicular material is heated to high temperatures ($T > 5 \times 10^5$ K), it would be very useful to obtain simultaneous high resolution observations of line profiles and Doppler shifts in spectral

lines formed at chromospheric, transition region in coronal temperatures. The desired spatial resolution is < 1" and the spectral resolution $\lambda/\Delta\lambda > 3 \times 10^4$. This can be achieved with a suitably designed EUV instrument.

7. SOLAR FLARES AND SURGES

In order to obtain additional insights concerning the nature of the different types of impulsive phenomena discussed above, we analyzed EUV observations of several subflares observed in the McMath region 12628. Figure 24 presents a series of four pairs of O VI and Mg X spectroheliograms of one of these subflares. Each pair of spectroheliograms was acquired simultaneously along with spectroheliograms in four other spectral lines not shown. Time progresses from bottom to top with the interval between spectroheliograms being 5.5 minutes. The subflare occurred at the base of the loops in the active region in the foreground. In the Mg X spectroheliograms (right hand set of pictures) the subflare is visible as a small bright patch near the bottom of the pictures. The event grows in size and in intensity in the middle two spectroheliograms and then fades in intensity by the time of the last spectroheliogram (top spectroheliogram in the sequence). At the flare site all of the EUV spectral lines observed (Ly α, C II, C III, O IV, O VI, and Mg X) brighten simultaneously within the 5.5 minutes temporal resolution of the data. This is shown for three of the lines in Figure 25 (left-hand plots) Lyman α λ1216 (from the chromosphere, $T \simeq 2 \times 10^4$ K), O VI λ1032 (from the transition region, $T \simeq 3 \times 10^5$ K) and Mg X λ625 (from the corona, $T \simeq 1.5 \times 10^6$) which shows intensities measured at the location of the subflare. The first large peak corresponds to the flare pictured in Figure 24. The second peak is due to a second subflare which occurred later at the same location.

The contrast in the photographic representations of the O VI spectroheliograms in Figure 24 is such that the enhanced intensities associated with the subflare (which occur in the same location as in Mg X) are not readily apparent. However, in O VI several mass ejections or surges associated with the flare are readily seen as "jets" extending to the left of the flaring region. If one compares the various spectroheliograms in the figure, one observes ejected material moving out along several different trajectories, presumably guided by the magnetic fields in the region. Note in particular (1) the very bright ejection that is at an angle of about 40 degrees to the horizontal, (2) the ejected material apparently falling downward on a curved trajectory near the top left of the active region (see upper-most spectroheliogram) and (3) the ejecta moving towards the bright point to the left of the tip of the brightest surge in the middle O VI spectroheliograms. The intensity of this bright point varied with time, apparently due to the infall of ejecta from the flare. The velocities of the ejecta appear to range between approximately 50 and 300 km per second.

One of the most interesting characteristics of these surges is that, although they are clearly visible in the chromospheric and transition region lines, they produce no measurable enhancement in the Mg X coronal line. The comparison of the Mg X and O VI images in Figure 24 illustrates this behavior. Figure 25 (right-hand plots) shows the

corresponding "light curves" for the flare region (bottom graph) and the bright surge to the left of the flare site (upper 3 plots). Note that the Lyman α and O VI intensities continue to increase after flare maximum, while the Mg X intensity declines. The decline in the Mg X emission is most likely due to Lyman continuum absorption from the cool material in the surge which may have appreciable optical thickness at λ625.

These observations suggest that no significant amount of material in the surge are raised to coronal temperatures ($T > 10^6$ K). (Material at coronal temperatures could be present under the unlikely circumstance that all of the hot material is shielded from view by the cool Lyman absorbing material. However, surges are also bright in O IV λ554 emission which is nearly as susceptible to the effects of Lyman continuum absorption as emission at λ625). This finding suggests that the mechanism responsible for the mass ejections or surges delivers most of the energy to driving the mass flows. The amount of energy involved with heating the ejected material is insufficient to raise the temperature of significant amounts of material to values above 10^6 K. There is, however, sufficient plasma heating to raise some of the material to transition region temperatures ($3 \times 10^4 < T < 10^6$ K) resulting in strongly enhanced emission in spectral lines formed at these temperatures.

8. CORONAL HEATING IN POLAR PLUMES

Polar plumes are ray-like structures that were first observed in white light eclipse photographs of the corona. Subsequent observations at EUV, XUV and x-ray wavelengths showed that these features are associated with coronal bright points which are observed to lie at the bases of the plumes. Analyses of the short-wavelength observations have shown that a substantial fraction of the mass in polar coronal holes apparently is contained in plumes. If this is the case, it is possible that plumes provide a substantial fraction of the mass flux in high speed solar wind streams originating in coronal holes (Ahmad and Withbroe 1977, Ahmad and Webb 1978). More recently, Ahmad and Mullan (1980) suggested that the mass flowing outward in plumes may be driven by magnetic forces of an impulsive nature.

In order to place empirical constraints on this and other acceleration and/or plasma heating mechanisms, we measured the variability of the O VI λ1032 and Mg X λ625 emission in the same three polar plumes used by Ahmad and Withbroe for constructing temperature-density models. We found that the coronal emission from three plumes (which were observed with approximately 1.7 minute temporal resolution over a period of about 40 minutes) exhibited only small ($\lesssim 10\%$) fluctuations in EUV emission over the observing period. This implies that temporal variations in the density and/or temperature were 5% or less. It also suggests that plumes are heated primarily by a quasi-steady state process. Although the variations in the measurements of the EUV emission from the plumes were small, they appear to be statistically significant. Two plumes decreased in brightness by approximately 10% during the 40 minute period of observations. In addition two plumes exhibited short-term (few minute) variations which appear to be due to small ($\sim 2 \times 10^4$ K) fluctuations in temperature caused by fluctuations in the local plasma

heating rate. If these features are a significant source of the mass flux in high speed solar wind streams originating in polar coronal holes, then the energy delivered to the plasma flowing out of these features is more likely from a steady-state process (e.g. Alfven or MHD fast mode wave heating) than a stochastic process, unless the energy inputs by the latter are delivered sufficiently frequently and regularly (time scale < minutes) to provide quasi-steady state heating and mass acceleration.

A coronal bright point at the base of one of the plumes was found to have a small enhancement or "flare" in brightness. There was no corresponding effect observed in the overlying plume. This difference in behavior could be due to the fact that the bright point most likely had a closed magnetic configuration which confined the "activity" to low-lying magnetic loops without causing significant effects in the overlying plume which most likely had an open magnetic configuration.

Additional studies of polar plumes are required before one can determine whether or not they are a major source of the mass flux in high speed solar wind streams that are believed to flow out of polar coronal holes. Of particular interest are long term studies of the emission (both spectral line and broad-band white light) and measurements of flow velocities, if any, using newly developed techniques such as Doppler-dimming of resonance lines (see review by Withbroe et al. 1983).

9. SUMMARY AND CONCLUSIONS

The findings of the various studies discussed in this report suggest the following scenario: The rapid release of energy in the low corona usually results in plasma heating in not only the corona, but also in the transition region and upper chromosphere. This is evidenced by the strong correlation found between localized energy releases in active regions and bright point flares which produce nearly simultaneous increases in the intensities of chromospheric, transition region and coronal lines. If the energy release results in the ejection of chromospheric material (either due to the energy release occurring in the chromosphere or perhaps due to energy transferred to the chromosphere from an energy release site in the corona), then the ejected material often is apparently not heated to coronal temperatures. Note we are distinguishing here between ejection of chromospheric material in bulk flows as opposed to the "evaporation" or "boiling" off of chromospheric material by energy transported from the corona. The intensities of coronal lines appear to be sensitive primarily to energy releases that result in heating of plasma to coronal temperatures, while the intensities of the chromospheric and, especially transition region lines are sensitive to energy releases that produce mass ejections and/or plasma heating. The observed temporal variability of transition region emission, which occurs over a much greater extent of the solar surface in both quiet and active regions than is the case for coronal lines, suggests that impulsive energy releases that cause mass ejections are a more frequent and widespread phenomena than impulsive energy releases that produce heating of plasma to coronal temperatures.

One can summarize our findings on the behavior of the EUV emission

from loops in magnetic bipolar regions in the following way: In small regions (spatial extent < 1') the EUV variations suggest that impulsive heating at chromospheric and coronal levels appears to be very important, possibly the dominant form of heating. The mechanism most likely evolves rapid release of magnetic energy, possibly associated with the emergence of magnetic flux from lower levels into the chromosphere and corona. In larger scale (>1') magnetic bipolar regions, there is evidence for both quasi-steady and impulsive heating, with quasi-steady heating dominating. This heating could be caused by either a mechanism such as steady-state current dissipation, or by a stochastic processe whose integrated effect (resulting from the smoothing caused by finite radiative and conductive cooling times) yields a nearly constant radiative output. The widespread variability of the emission in spectral lines formed at transition region temperatures ($10^5 < T < 10^6$ K) provides evidence that impulsive energy releases are a common, nearly continuous phenomenon in bipolar magnetic regions. However, at the present time we do not know what fraction of the total energy deposition in the atmosphere (chromosphere and low corona) originates in impulsive phenomena.

Our present results suggest that stochastic mechanisms may play an important role in heating the solar atmosphere at chromospheric and coronal levels. As has been suggested several times in this report these mechanisms most likely involve the rapid release of magnetic energy. It is possible that they are identical to mechanisms responsible for the energy release in flares. More study of existing data such as the Skylab, UV, EUV and X-ray observations are needed to provide additional information on the variability of the chromospheric, transition region and coronal emissions from different types of regions, particularly regions of different sizes and in different stages of evolutionary development. This can provide additional insights as to the importance of impulsive heating mechanisms, the location of energy deposition, and the magnitude of the energy delivered to the plasma by such mechanisms. Observations with more sophisticated instruments capable of measuring line profiles could yield invaluable information about mass flows and the dynamics associated with plasma heating and/or deposition of momentum thereby providing additional constraints on energy release mechanisms. Of particular interest from the ground are simultaneous high resolution (~1") measurements of velocities and magnetic fields in the photosphere and chromosphere, intensities of chromospheric lines such as He I λ10830, and VLA measurements of the radio emission from higher temperature plasma in overlying coronal loops. Such observations could help elucidate possible relationships between magnetic field emergence and plasma heating in the upper chromosphere and low corona.

One scientific paper resulting from the studies reported here has been published (Withbroe 1983a on results presented in Section 6). A second paper has been submitted for publication (Withbroe 1983b on results presented in section 8). Several other papers are in preparation (on Sections 2-5, 7). In addition to the Principal Investigator, the following participated in the various aspects of the study: Dr. S. R. Habbal, Dr. R. H. Levine, R. Ronan, B. Toth and C. Zapata.

10. REFERENCES

Ahmad, I. A. and Mullan, D. J. 1980, Bull. Amer. Astron. Soc. **12**, 918.

Ahmad, I. A. and Webb, D. F. 1978, Solar Phys. **58**, 323.

Ahmad, I. A. and Withbroe, G. L. 1977, Solar Phys. **53**, 397.

Athay, R. G. 1976, The Solar Chromosphere and Corona: Quiet Sun, (D. Reidel, Dordrecht, Holland).

Athay, R. G. and Holzer, T. E. 1982, Astrophys. J., **255**, 743.

Athay, R. G. and White, O. R. 1978a, Astrophys. J. Suppl., **39**, 333.

Athay, R. G. and White, O. R. 1978b, Astrophys. J., **226**, 1135.

Beckers, J. M. 1968, Solar Phys., **3**, 367.

Beckers, J. M. 1972, Ann. Rev. Astron. Astrophys., **10**, 73.

Bohlin, J. D., Vogel, S. N., Purcell, J. D., Sheeley, N. R., Jr., Tousey, R. and Van Hoosier, M. E. 1975, Astrophys. J., **197**, L133.

Cox, D. P. and Tucker, W. H. 1969, Astrophys. J., **157**, 1157.

Dupree, A. K., 1972, Astrophys. J., **178**, 527

Habbal, S. R. and Withbroe, G. L. 1981, Solar Phys. **69**, 177.

Hollweg, J. V., Jackson, S. and Galloway, D. 1982, Solar Phys., **75**, 35.

Pneuman, G. W. and Kopp, R. A. 1978, Solar Phys., **57**, 49.

Raymond, J. C., Cox, D. P. and Smith, B. W. 1976, Astrophys. J., **204**, 290.

Reeves, E. M., Timothy, J. G. and Huber, M. C. E., 1977a, Applied Optics, **16**, 837.

Reeves, E. M., Timothy, J. G., Huber, M. C. E. and Withbroe, G. L. 1977b, Applied Optics, **16**, 849.

Rosner, R., Tucker, W. H. and Vaiana, G. S. 1978, Astrophys. J., **220**, 643.

Shibita, K. 1982, Solar Phys. **81**, 9.

Sturrock, P. A. (ed.) 1980, Solar Flares, (Colo. Assoc. Univ. Press, Boulder).

Tucker, W. H. 1973, Astrophys. J. **186**, 285.

Vaiana, G. S. and Rosner, R. 1978, Ann. Rev. Astron. Astrophys., 16, 393.

Vernazza, J. E., Avrett, E. H. and Loeser, R. 1981, Astrophys. J. Suppl., 45, 636.

Wentzel, D. 1981, in The Sun as a Star, NASA SP-450, S. Jordan, ed. (NASA), p331.

Withbroe, G. L. 1981, in Active Regions, F. Q. Orrall, ed., (Colo. Assoc. Univ. Press, Boulder), p199.

Withbroe, G. L. 1983a, Astrophys. J., 267, 825.

Withbroe, G. L. 1983b, submitted to Solar Phys..

Withbroe, G. L., Jaffe, D. T., Foukal, P. V., Huber, M. C. E., Noyes, R. W., Reeves, E. M., Schmahl, E. J., Timothy, J. G. and Vernazza, J. E. 1976, Astrophys. J., 203, 528.

Withbroe, G. L., Kohl, J. L., Weiser, H., and Munro, R. H. 1983, Space Sci. Rev., in press.

Withbroe, G. L. and Mariska, J. T. 1976, Solar Phys., 48, 21.

Withbroe, G. L. and Noyes, R. W. 1977, Ann. Rev. Astron. Astrophys., 15, 363.

TABLE 1. EUV SCALE HEIGHTS

Identification	λ (Å)	log T	Scale Height H_S		
			Equatorial Quiet Region	Polar Quiet Region	Polar Coronal Hole
HI Lyman C	814	4.0	-	2000 ± 300	1900 ± 300
HI Lyman α	1216	4.3	2200 ± 300	2200 ± 300	2200 ± 300
C II	1335	4.65	2200 ± 300	2200 ± 300	1800 ± 300
C III	977	4.95	1900 ± 300	1800 ± 300	2000 ± 300
O IV	554	5.3	2000 ± 300	2000 ± 300	2000 ± 300
O VI	1032	5.5	-	-	-
Ne VIII	465	5.8	-	-	-
Mg X	625	6.15	-	-	-

11. FIGURES

Fig. 1.--A (5' x 5') Mg X spectroheliogram showing the bright points studied by Habbal and Withbroe (1981). Since the instrument used a photoelectric detection system, the primary data are in digital form. This picture was produced from the digital data using a computer driven cathode ray tube display. Progressively lighter shades of gray correspond to increasing intensities.

Fig. 2.--EUV spectroheliograms of bright points in six different spectral lines: the chromospheric Lyman α and C II lines, the chromospheric-coronal transition region C III, O IV and O VI lines and the coronal Mg X line. The feature circled (BP6) shows how a bright point appears in those different EUV lines. The larger bright area immediately below BP6 is the small active region discussed in Section 3. East is toward the top, north to the right.

Fig. 3.--Total intensity (counts/0.04 second) and areal extent (5" x 5" pixels) changes with time measured in Mg X for BP3 (see Habbal and Withbroe 1981).

Fig. 4.--Upper graph: Intensity variation in Mg X (counts/0.04 second) as a function of time (hours) for BP-A in a polar coronal hole. Lower graph: Intensity variation versus time showing only time-varying component of the intensity. (*The numbers in the label for the abscissa* are the coordinates of the pixels making up BP-A in the spectroheliogram.)

Fig. 5.--Upper graph: Intensity variation in O VI as a function of time for entire 25" x 40" area making up BP-A. Lower graph: Intensity variation in O VI for a small 10" x 15" area of BP-A.

Fig. 6.--Intensity as a function of time for BP-B as measured in Lyman α λ1216 (chromosphere), O VI λ1032 (transition region) and Mg X λ625 (corona).

Fig. 7.--Same as Fig. 6, but for BP-C.

Fig. 8.--Same as Fig. 6, but for BP-D.

Fig. 9.--Same as Fig. 6, but for BP-E.

Fig. 10.--Contour maps constructed from Mg X λ625 spectroheliograms showing some of the spatial and temporal changes in the small active region discussed in Section 3 (also see Fig. 1). The time (hr, min) that each spectroheliogram was acquired on August 21, 1973 are given. East is to the left, north toward the top. The contours were drawn at levels of 60, 90, 150 (shaded light gray), 230 (shaded dark gray) and 350 (shaded black) counts/integration time. The mean background level was approximately 3 counts in the coronal hole areas and 30 counts in the quiet regions (areas not in bright points, active regions or coronal hole). The contoured area is 100" x 55" with the tick marks at intervals of 5" (horizontally) and 2.5" (vertically). This area is in the upper right quadrant of Fig. 1 and 2 (note rotation of 90 degrees since east is at the top of Fig. 1 and 2) immeditately below BP-6.

Fig. 11.--Same as Fig. 10, but later in time.

Fig. 12.--Same as Fig. 10, but later in time.

Fig. 13.--Left hand plots: Variation of the total intensity in the eastern area of the small active region as a function of time for Lyman α (chromosphere), C III, O IV and O VI lines (transition region) and Mg X line (corona). The expected variations due to statistical fluctuations are smaller than the size of the data points. The dashed lines connect points during long intervals when there were no observations (usually due to spacecraft night). The intensity peaks at 0524 and 0603 are due to the subflares visible in Fig. 10. One unit on the ordinate corresponds to 0.04 dex. Right hand plots: Total intensities from western area of the small active region.

Fig. 14.--Spectroheliograms showing the appearance of McMath region 12628 (in foreground) and 12634 (on limb) in several EUV spectral lines. The Ly α, O VI and Mg X spectroheliograms were acquired simultaneously during a subflare (see Section 7). The C III spectroheliogram was acquired 5.5 minutes earlier and the Ne VII and Si XII spectroheliograms were acquired 1.5 hours earlier.

Fig. 15.--Intensity as a function of time measured in the O VI and Mg X lines at the left (left-hand plots) and right (right-hand plots) footpoints of the coronal loops in McMath region 12634 (see Fig. 14).

Fig. 16.--Mg X intensity as a function of time for four areas in the loops seen above the limb in McMath region 12634 (see Fig. 14).

Fig. 17.--Sub-flarelike intensity enhancements observed in the loops of McMath region 12628 (see Fig. 14).

Fig. 18.--Quiet solar limb area approximately 45° N of east obtained on 5 January 1974 at 2120 UT.

Fig. 19.--Intensity of CIII λ977 (measured in counts/0.040 s) plotted as a function of distance ρ (in solar radii) from sun-center (points). The measurements are from the quiet region shown in Fig. 18. Also plotted are intensities calculated with a model having no spicular contribution (dashed line), spicular contribution with H_s = 1900 km (solid line) and H_s = 2500 km (dotted line).

Fig. 20.--Intensities measured at several wavelengths in a polar coronal hole (points). The curves are for intensities calculated with the Withbroe-Mariska spicular model (see text).

Fig. 21.--Ratio σ_t/σ_e plotted as a function of position for measurements made along scan lines located at different mean distances ρ from sun-center. The measurements were acquired at 2.5" intervals along a 5' long scan line oriented parallel to the limb (see text). For each plot the value $\sigma_t/\sigma_e = 1$ is marked by a light horizontal line. Statistical noise is expected to produce variations in $\sigma_t/\sigma_e \simeq \pm 0.2$.

Fig. 22.--Ratio σ_t/σ_e plotted as a function of position for measurements

made in several spectral lines at $\rho \simeq 1.005$ ($h \simeq 3500$ km). Statistical noise is expected to produce variations in $\sigma_t/\sigma_e \simeq \pm 0.2$.

Fig. 23.--Ratio $\sigma_t(\rho)/\sigma_e(\rho)$ as a function of distance ρ from sun-center.

Fig. 24.--Spectroheliograms in O VI λ1032 (left-hand set of pictures) and Mg X λ625 (right-hand set of pictures). Each pair (row) of spectroheliograms was acquired simultaneously at intervals of 5.5 min. Time progresses from bottom to top. Subflare and associated surges are visible near the bottom of the pictures.

Fig. 25.--Left-hand plots: Intensity as a function of time in the area where the subflare shown in Fig. 24 occurred. Curves are given for Lyman δ, O VI λ1032 and Mg X λ625. The subflare shown in Fig. 24 caused the first intensity enhancement. The second peak was caused by a later subflare that occurred in the same region. Right-hand plots: Intensities in the region adjacent to the subflare where the surges are observed (area to left of subflare shown in Fig. 24). For comparison we have plotted (lowest curve) Lyman alpha intensity variation measured in the flaring region.

BRIGHT POINTS IN A CORONAL HOLE
AUG 21, 1973 05:35 UT
Mg x 625 Å

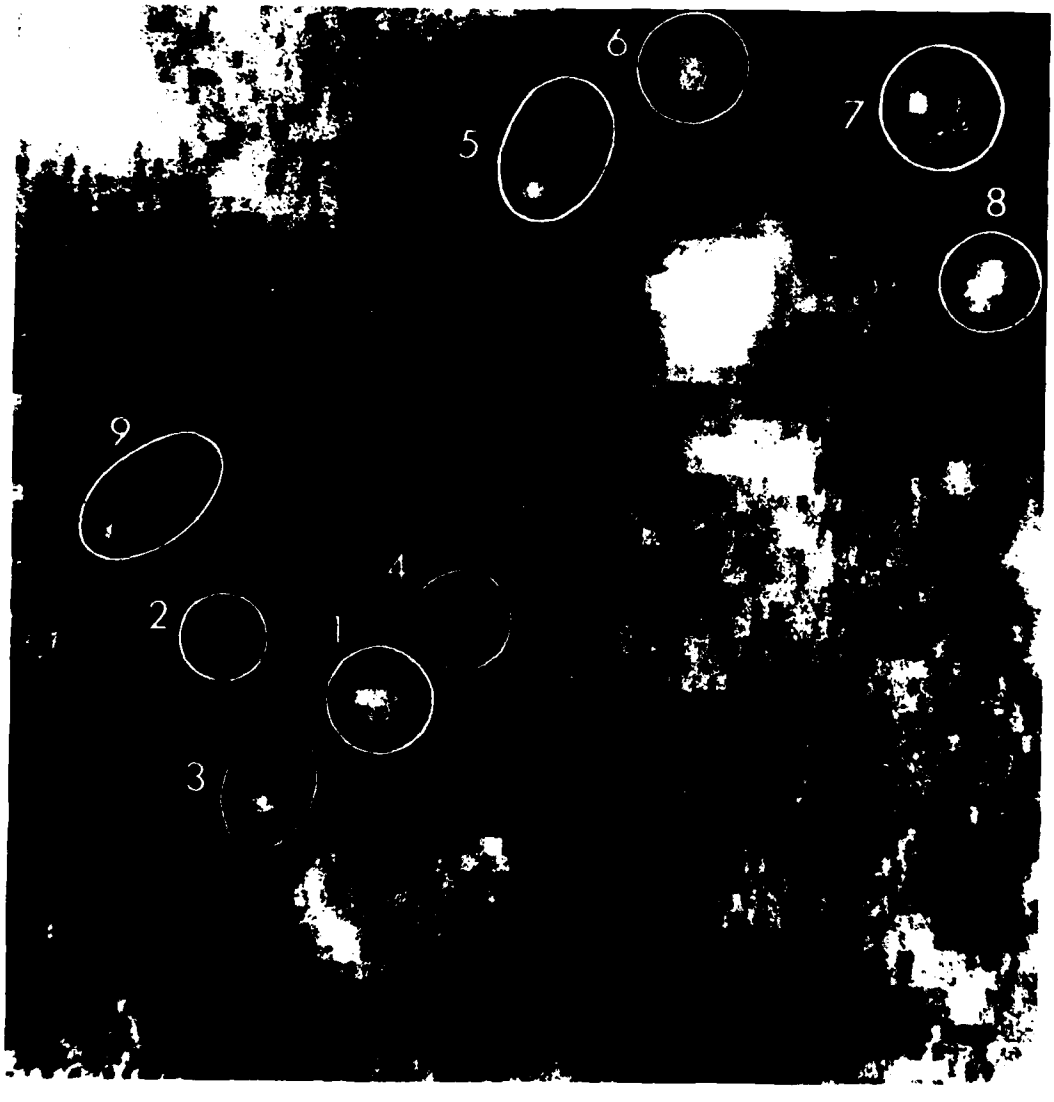

Figure 1

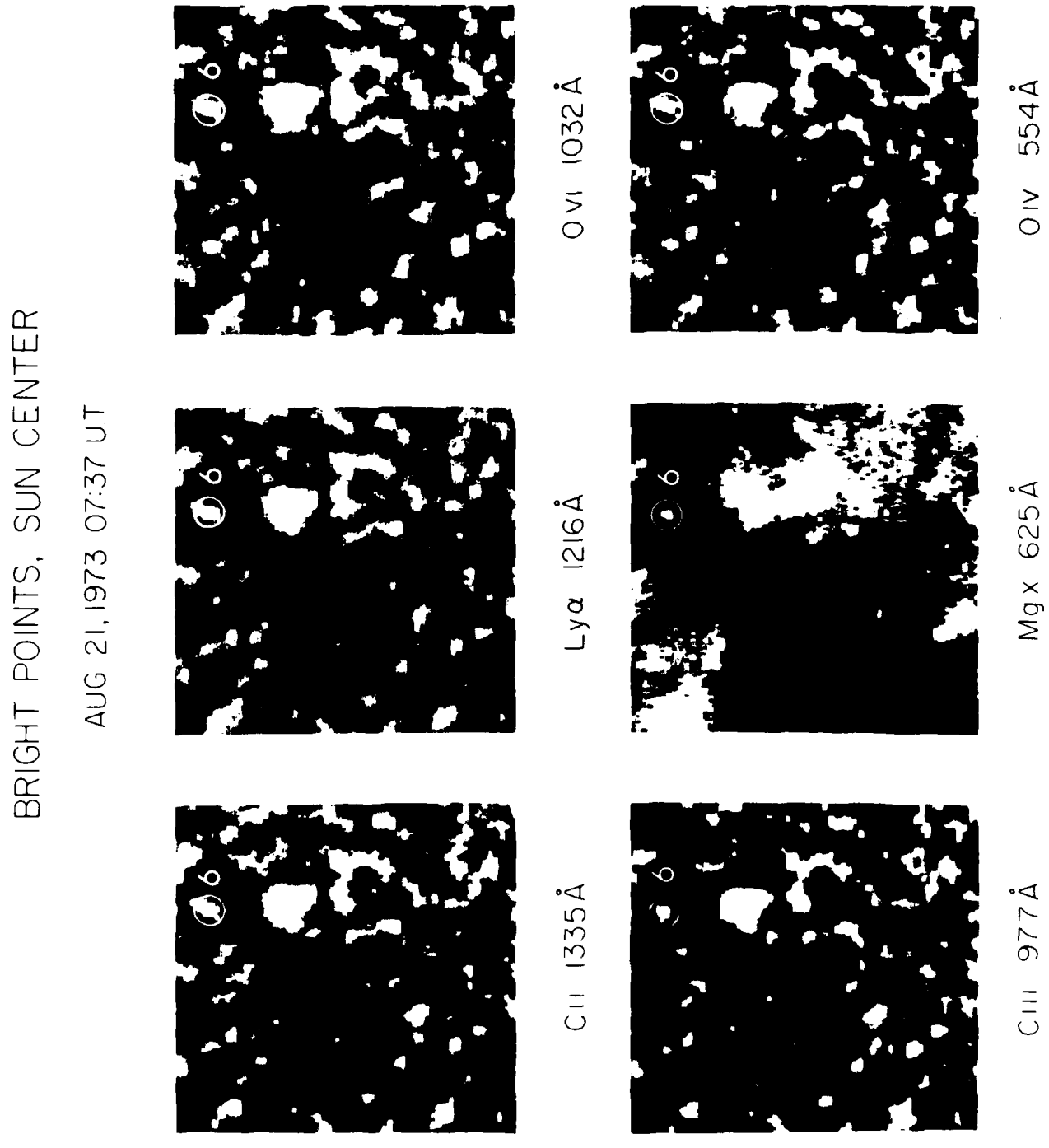
BRIGHT POINTS, SUN CENTER
AUG 21, 1973 07:37 UT
O VI 1032 Å
O IV 554 Å
Ly α 1216 Å
Mg X 625 Å
C II 1335 Å
C III 977 Å

Figure 2

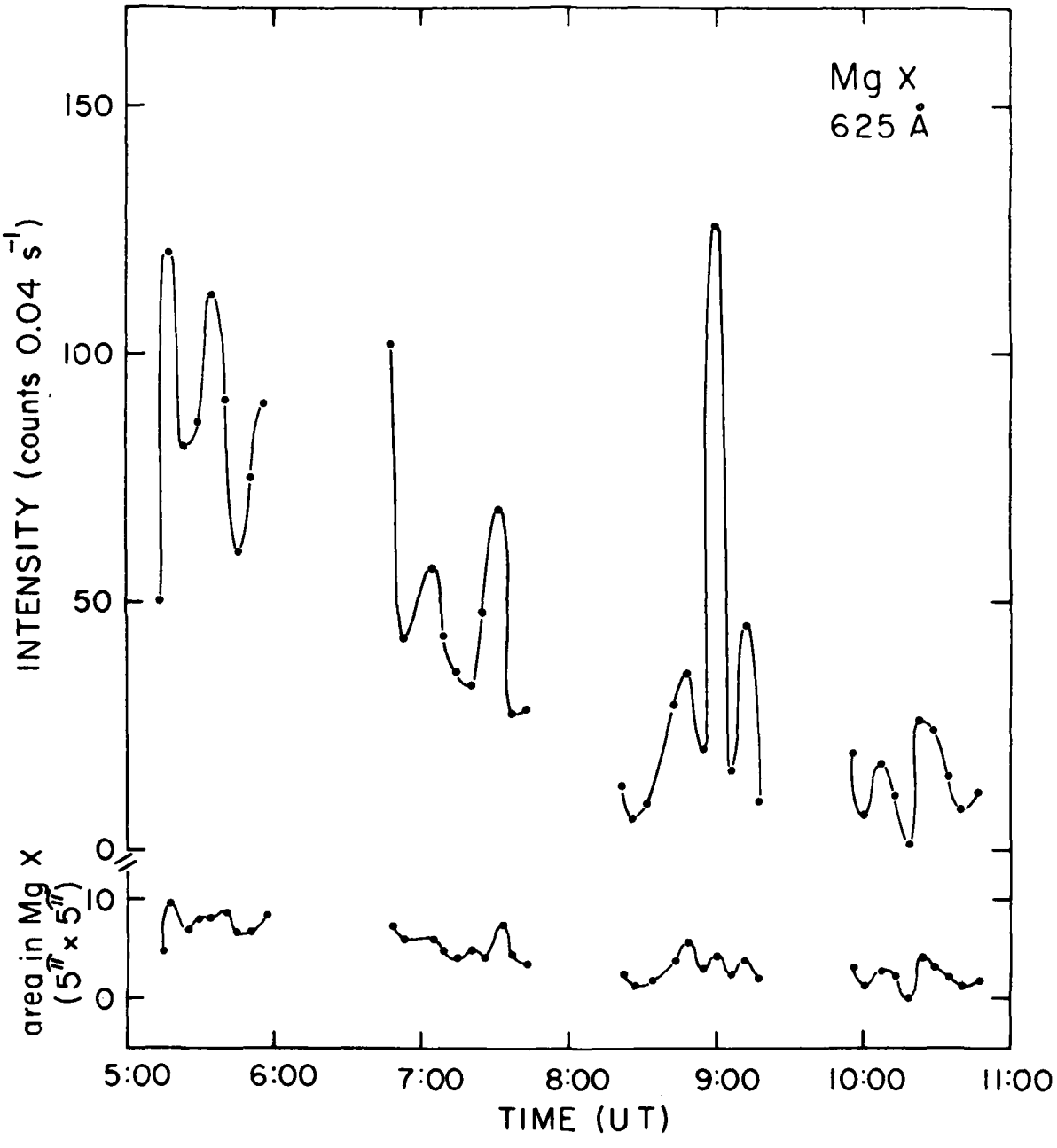
Mg X
625 Å
150
100
50
0
INTENSITY (counts 0.04 s⁻¹)
10
0
area in Mg X
(5″ x 5″)
5:00
6:00
7:00
8:00
9:00
10:00
11:00
TIME (UT)

Figure 3

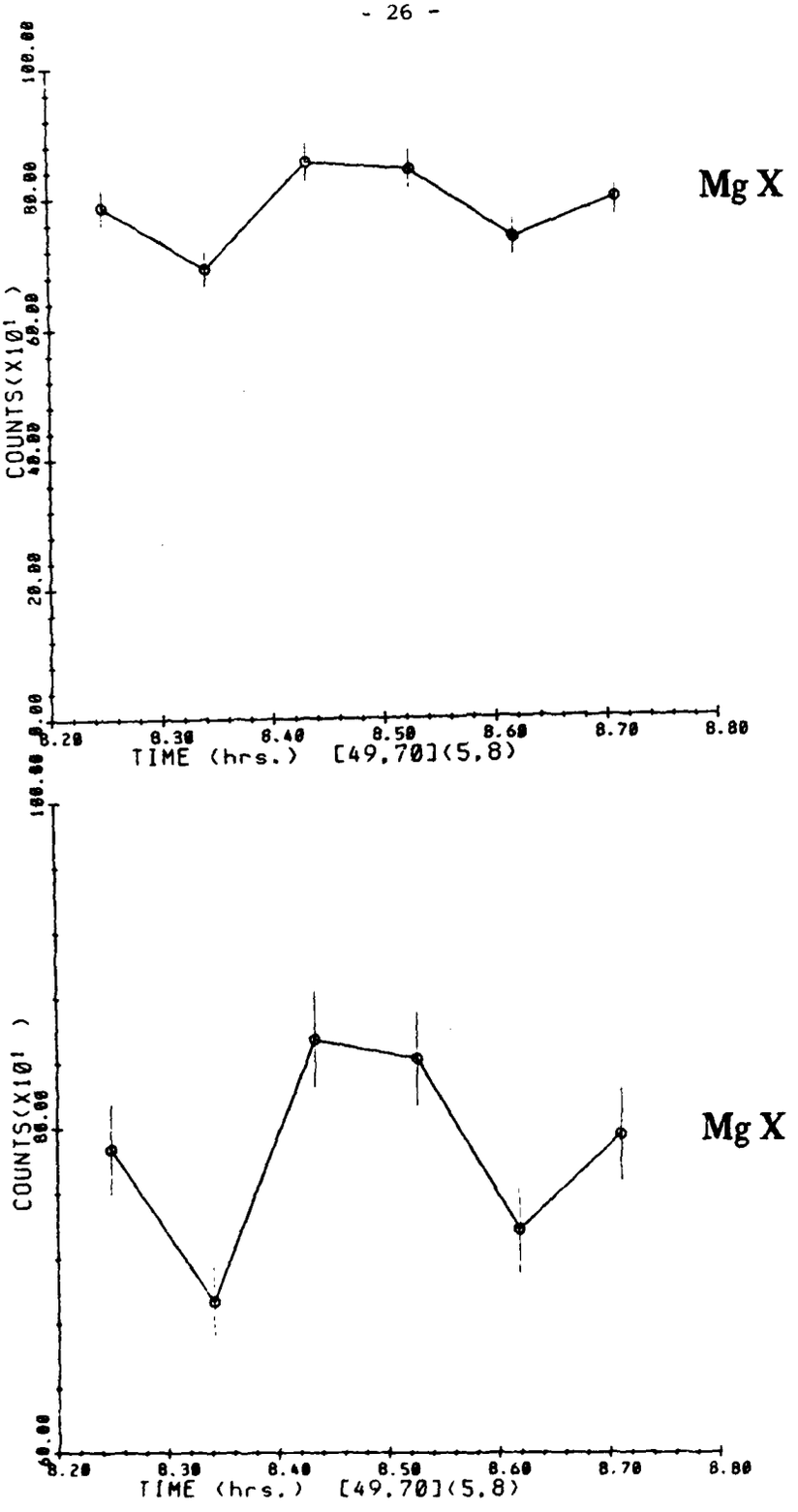
Mg X
COUNTS(X10¹)
100.00
80.00
60.00
40.00
20.00
0.00
8.20
8.30
8.40
8.50
8.60
8.70
8.80
TIME (hrs.) [49,70](5,8)
Mg X
COUNTS(X10¹)
80.00
0.00
8.20
8.30
8.40
8.50
8.60
8.70
8.80
TIME (hrs.) [49,70](5,8)

Figure 4

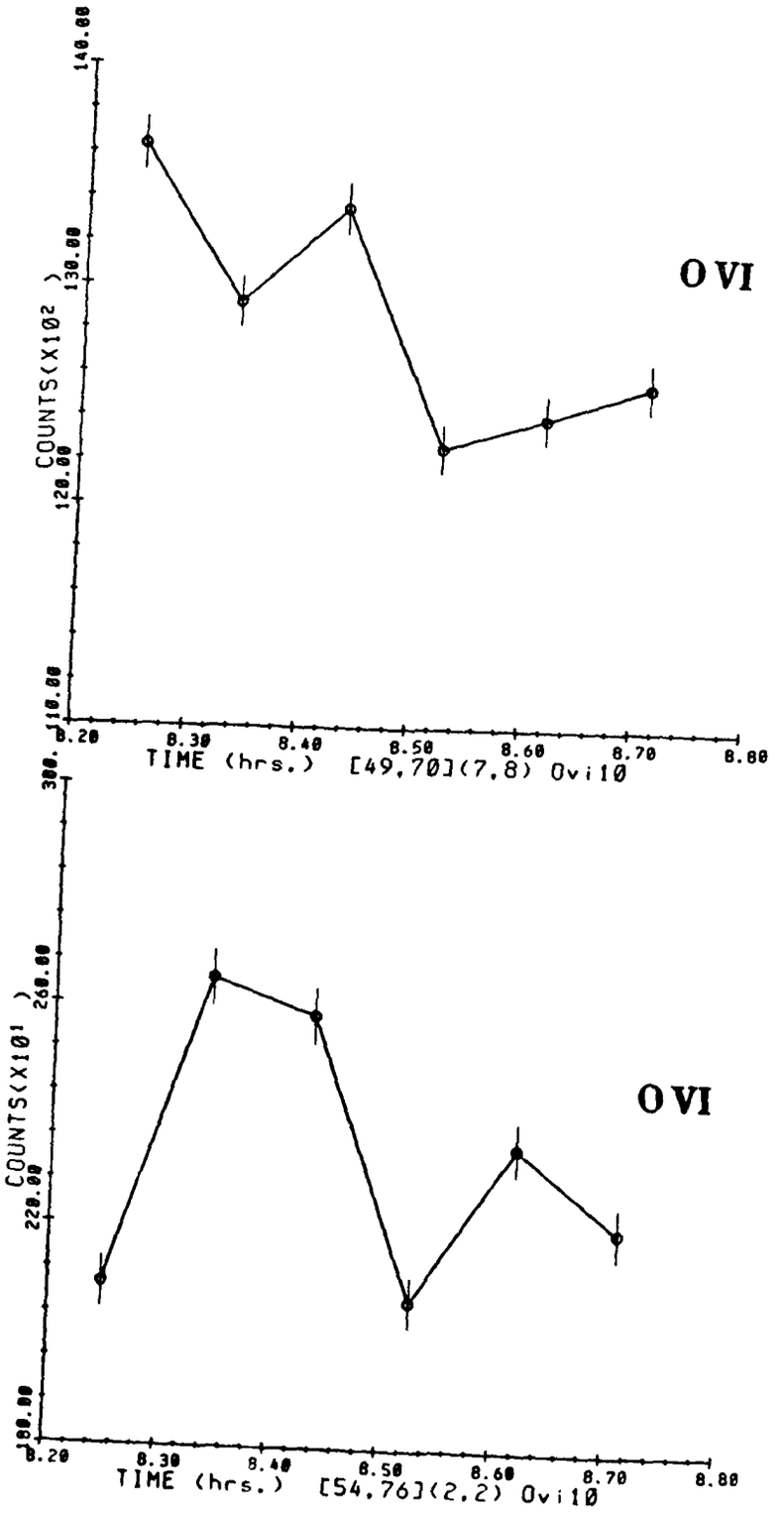
140.00
130.00
120.00
110.00
COUNTS(X10²)
OVI
8.20
8.30
8.40
8.50
8.60
8.70
8.80
TIME (hrs.) [49,70](7,8) Ovi10
300.
260.00
220.00
180.00
COUNTS(X10¹)
OVI
8.20
8.30
8.40
8.50
8.60
8.70
8.80
TIME (hrs.) [54,76](2,2) Ovi10

Figure 5

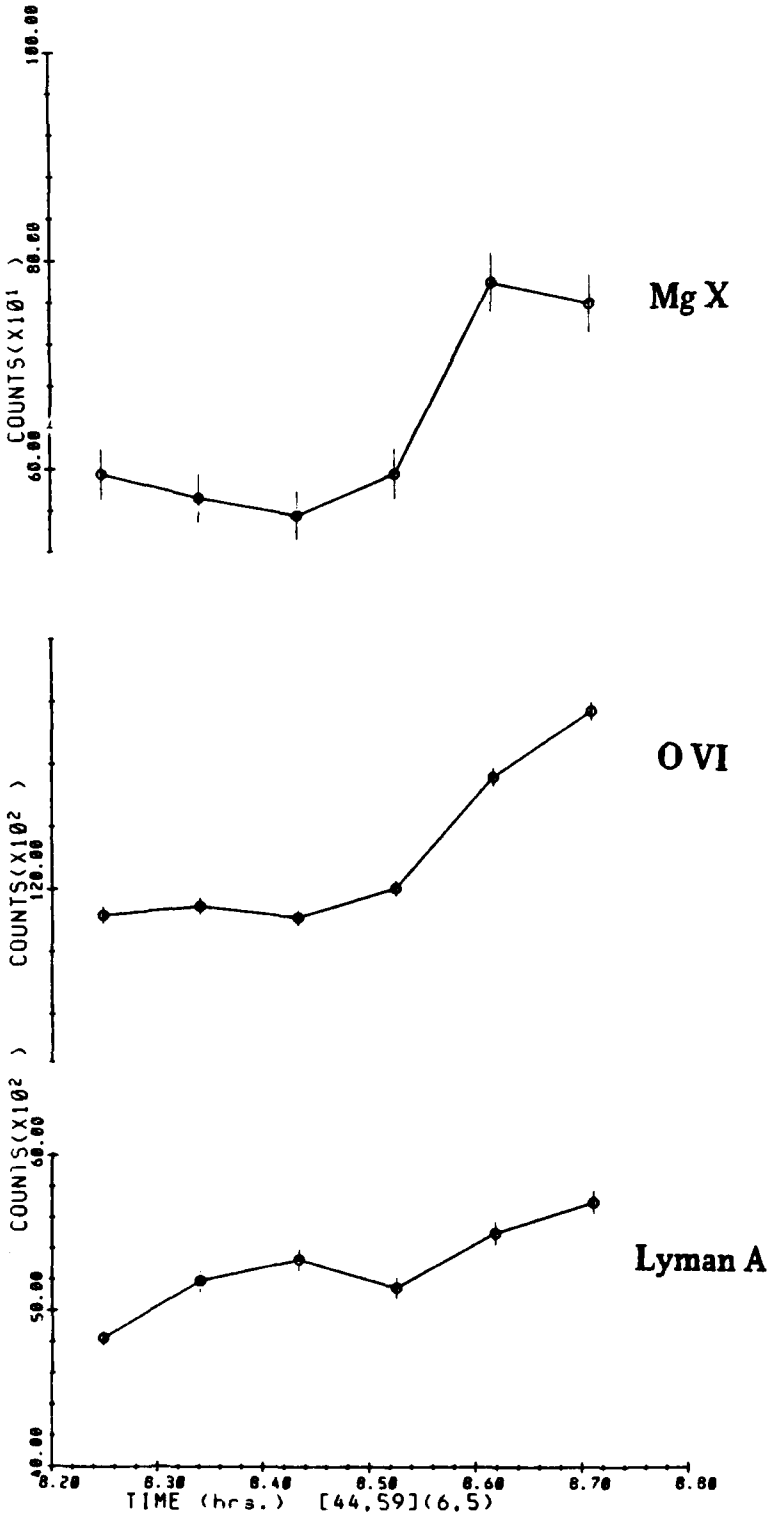
COUNTS(X10¹)
Mg X
COUNTS(X10²)
O VI
COUNTS(X10²)
Lyman A
8.20
8.30
8.40
8.50
8.60
8.70
8.80
TIME (hrs.) [44,59](6,5)

Figure 6

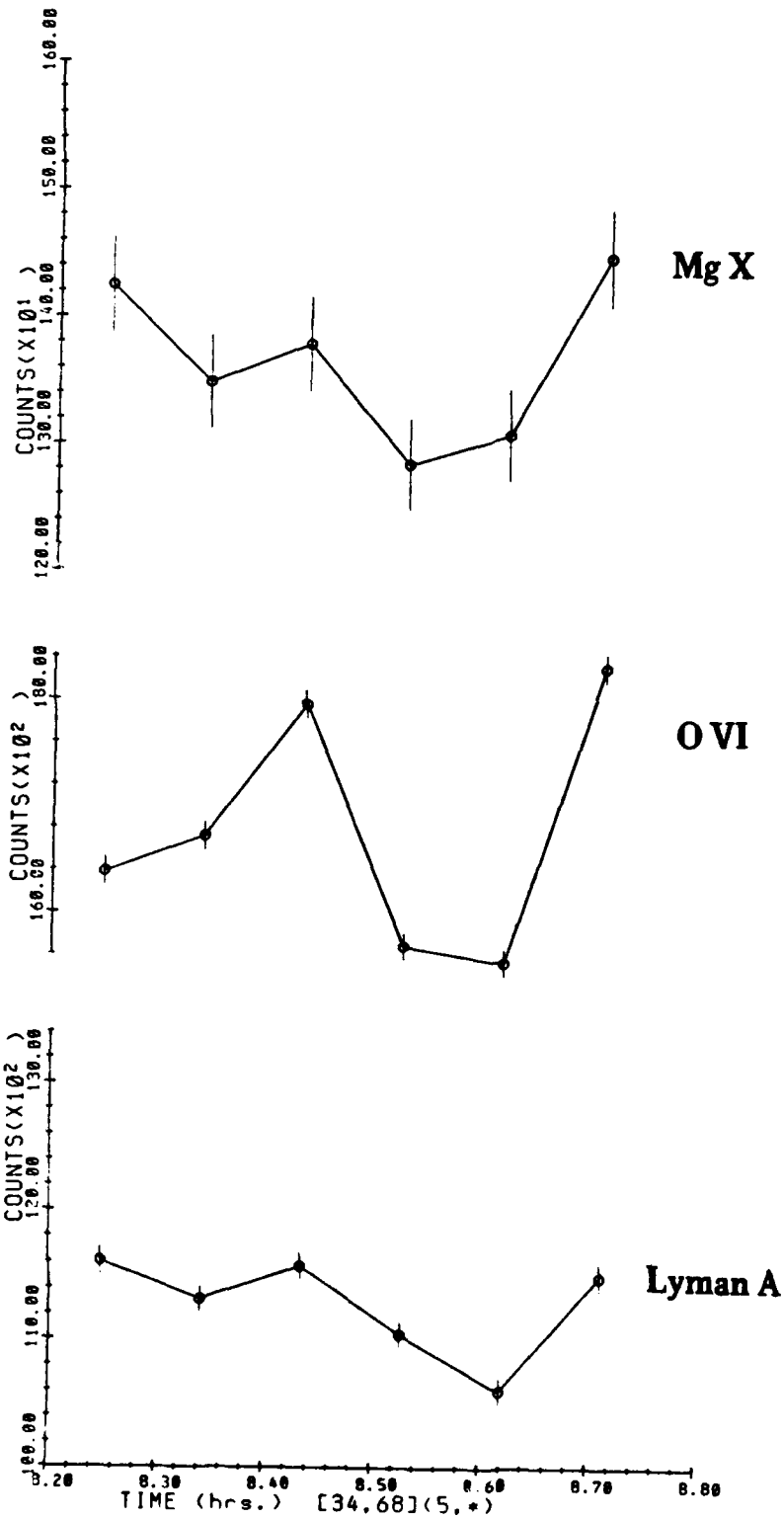
COUNTS(X10¹)
160.00
150.00
140.00
130.00
120.00
Mg X
COUNTS(X10²)
180.00
160.00
O VI
COUNTS(X10²)
130.00
120.00
110.00
100.00
Lyman A
8.20
8.30
8.40
8.50
8.60
8.70
8.80
TIME (hrs.) [34,68](5,*)

Figure 7

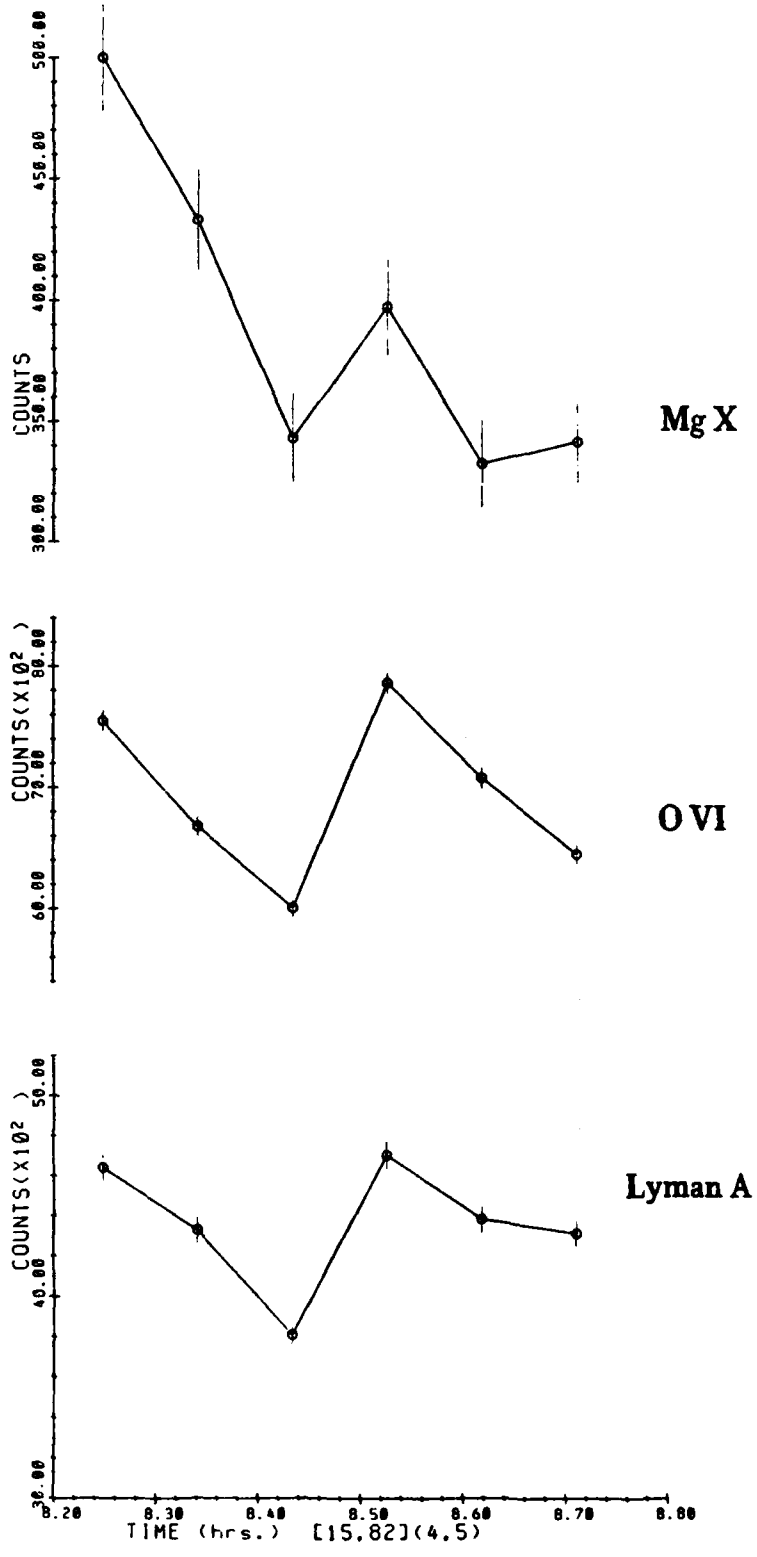
COUNTS
500.00
450.00
400.00
350.00
300.00
Mg X
COUNTS(X10²)
80.00
70.00
60.00
O VI
COUNTS(X10²)
50.00
40.00
30.00
Lyman A
8.20
8.30
8.40
8.50
8.60
8.70
8.80
TIME (hrs.) [15,82](4,5)

Figure 8

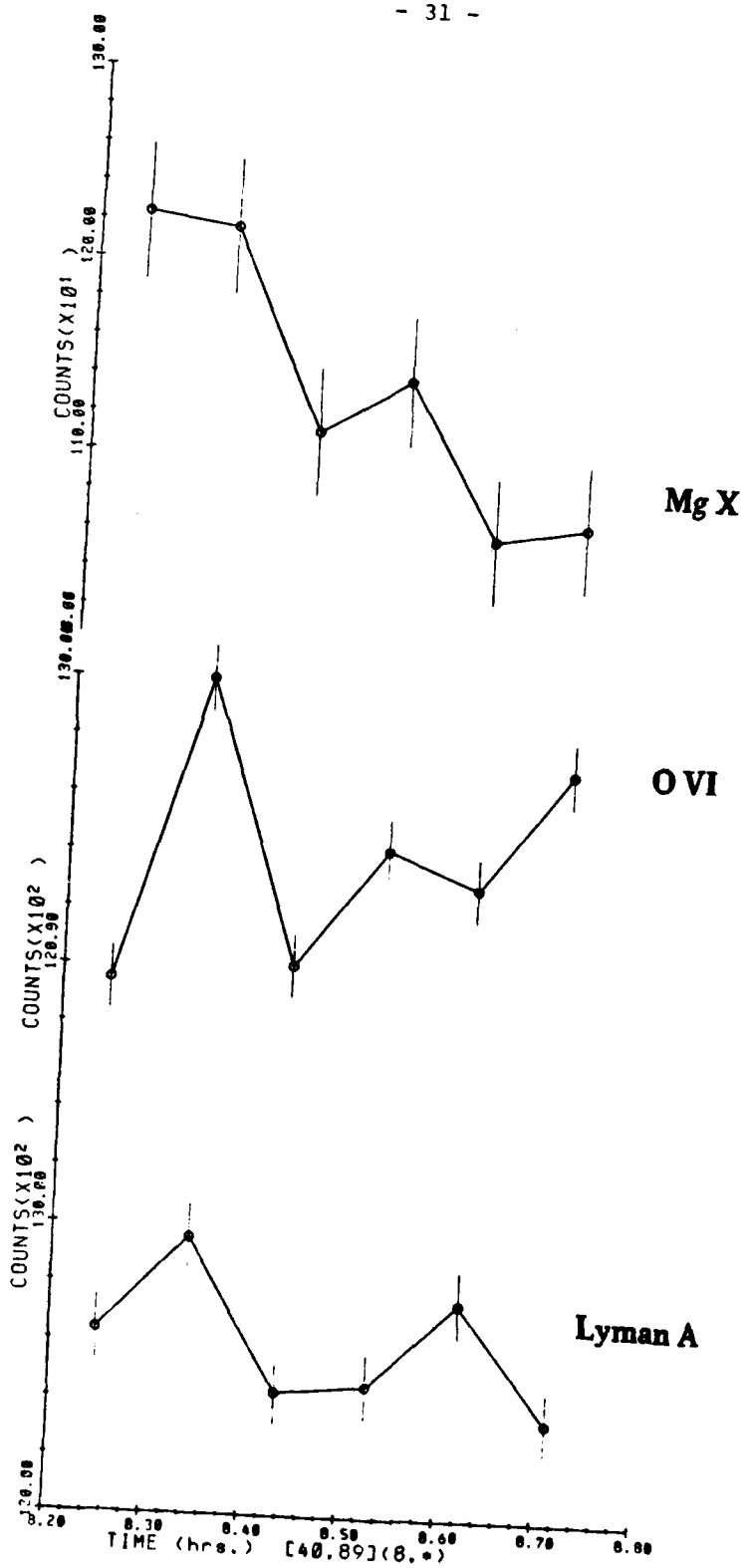
COUNTS(X10¹)
Mg X
COUNTS(X10²)
O VI
COUNTS(X10²)
Lyman A
TIME (hrs.)
[40,89](8,*)

Figure 9

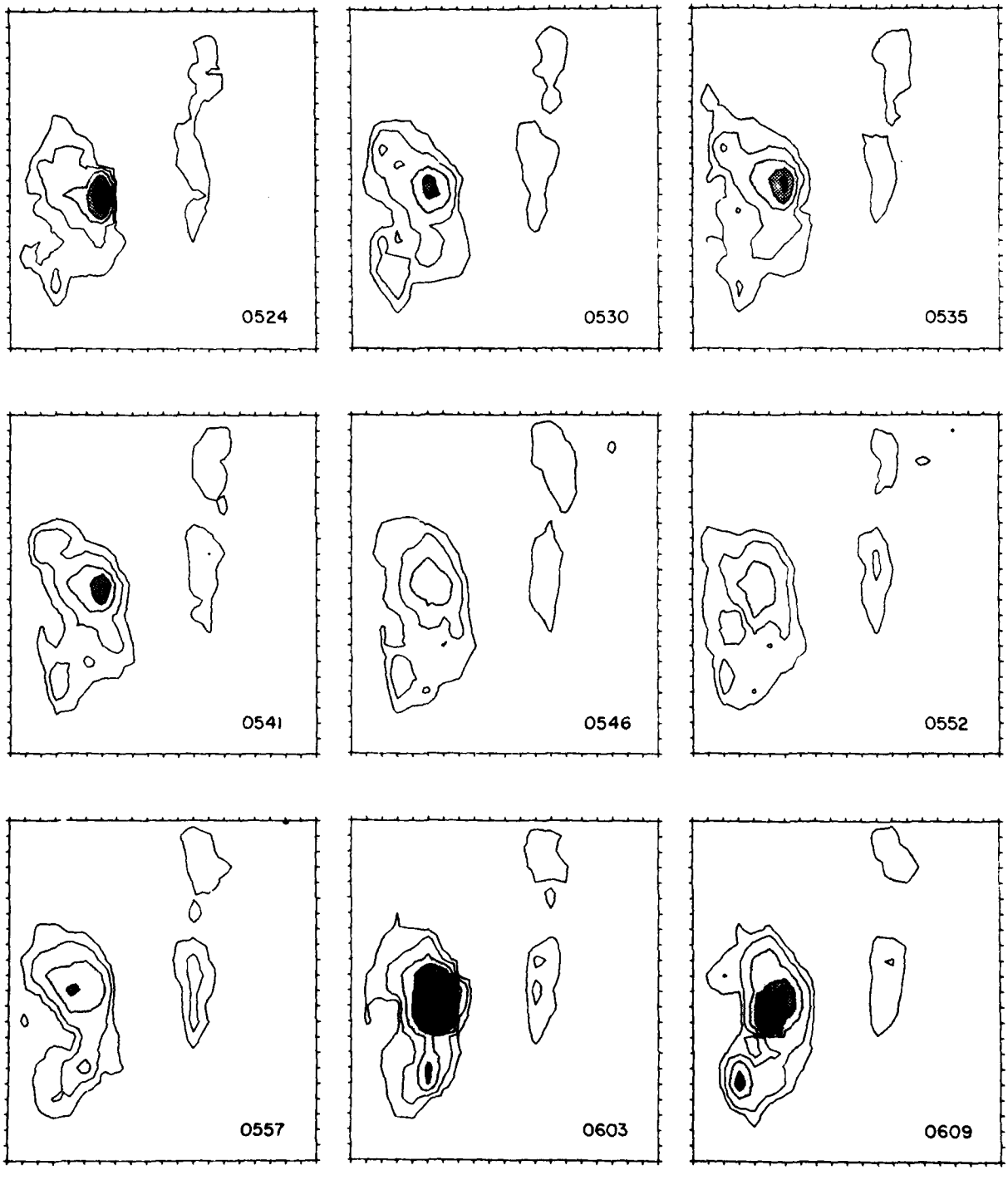

Figure 10

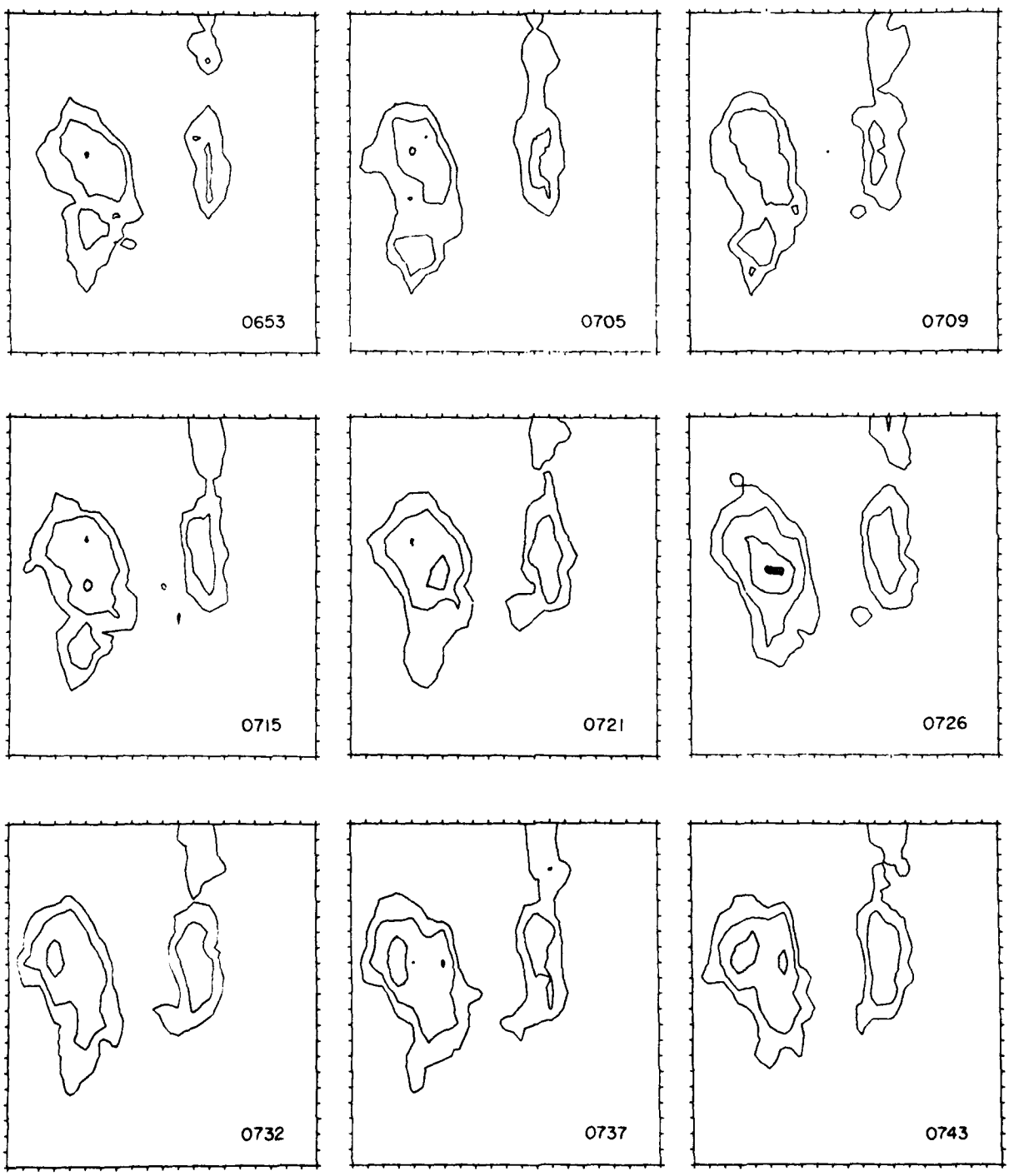

Figure 11

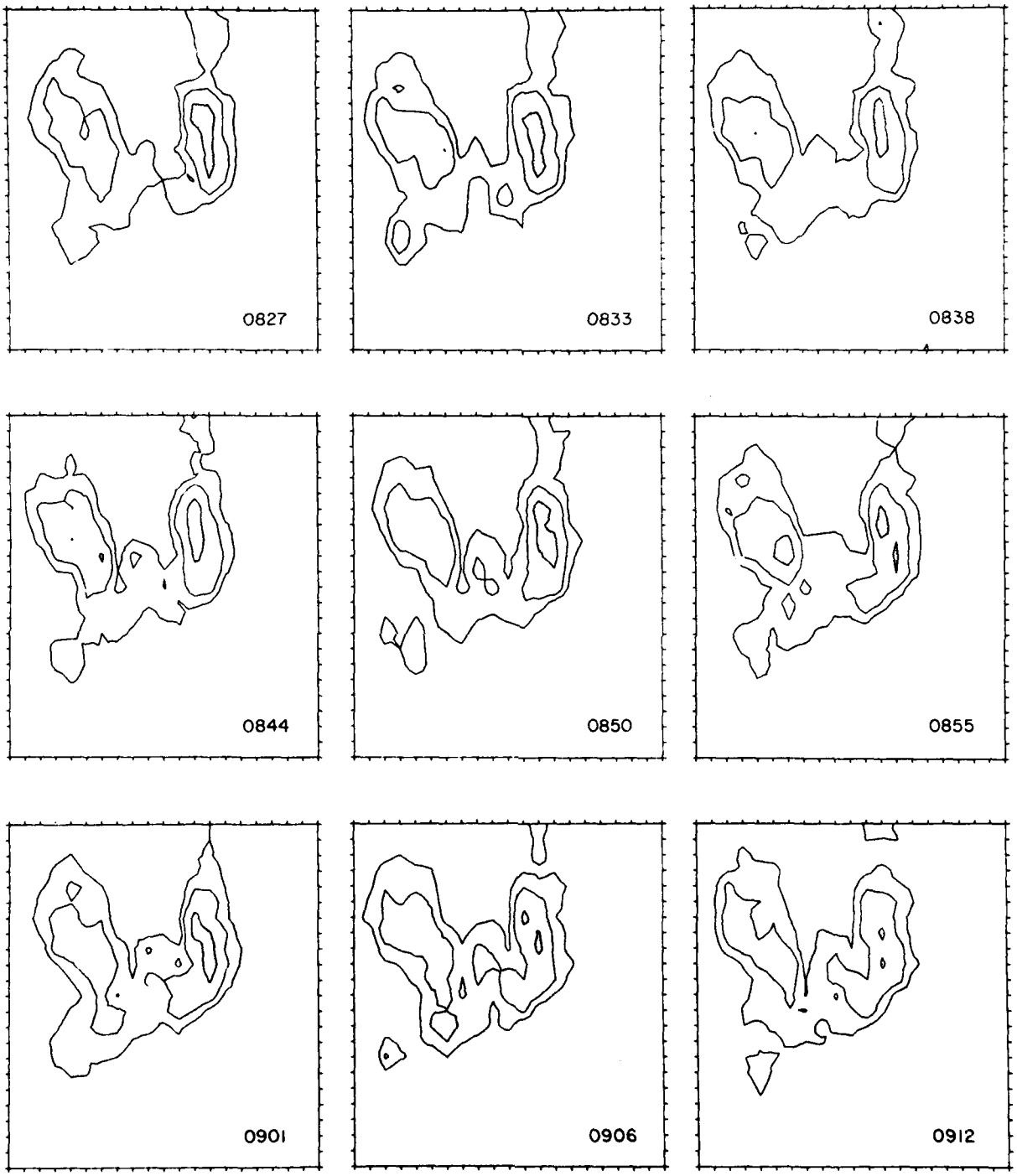

Figure 12

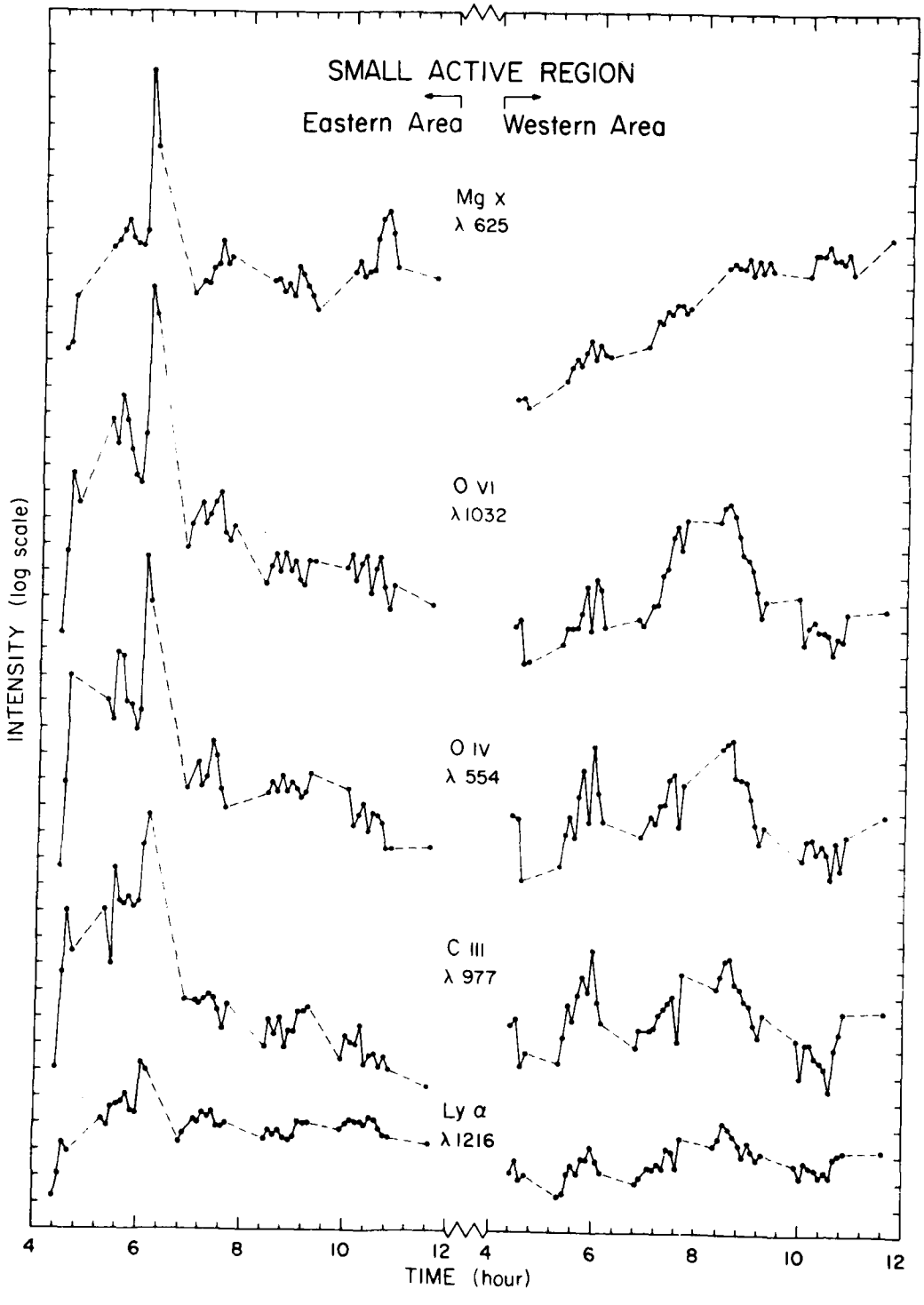
SMALL ACTIVE REGION
Eastern Area
Western Area
Mg X
λ 625
O VI
λ1032
O IV
λ 554
C III
λ 977
Ly α
λ1216
INTENSITY (log scale)
4
6
8
10
12
4
6
8
10
12
TIME (hour)

Figure 13

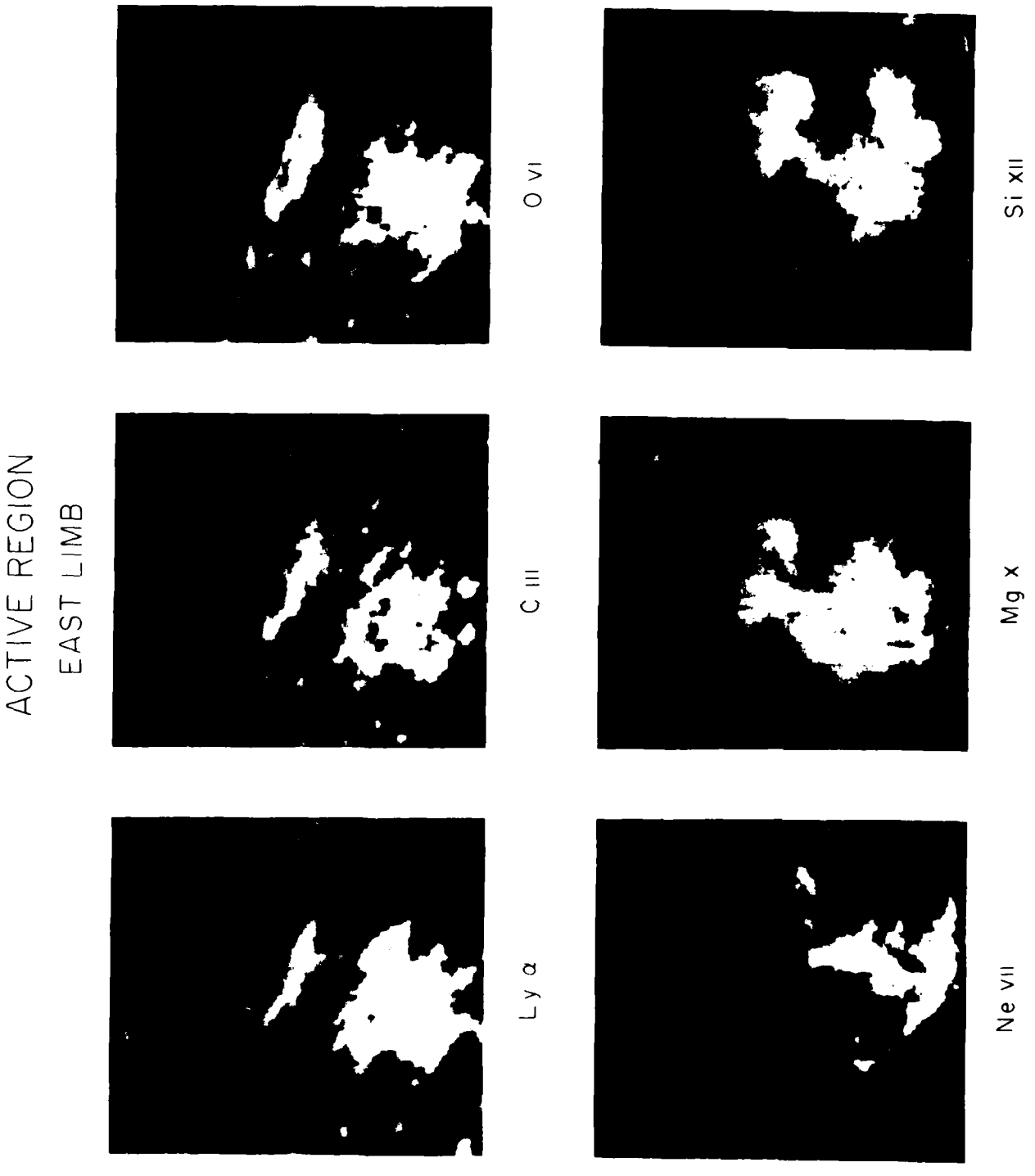

Figure 14

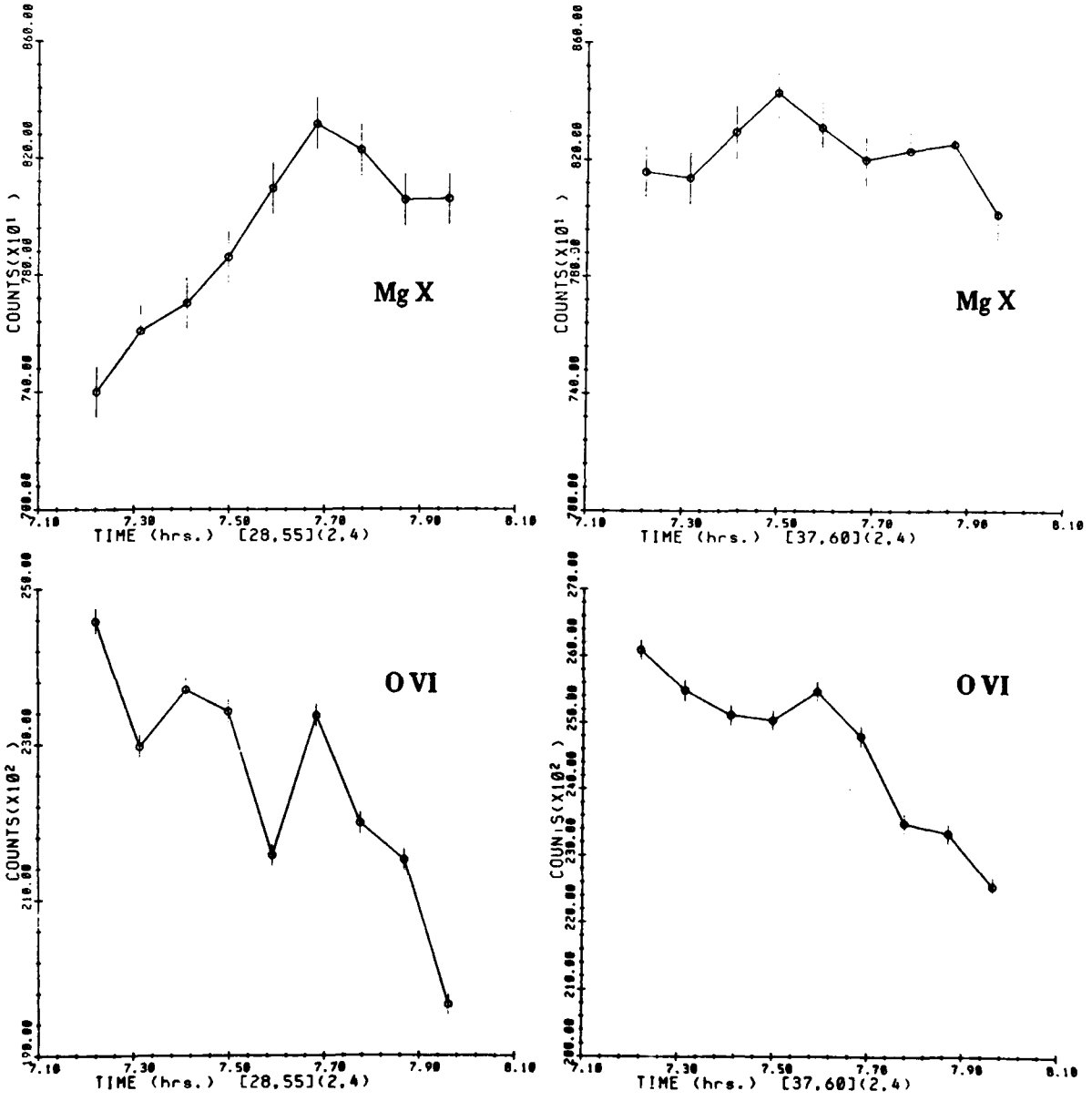
Mg X
COUNTS(X10¹)
TIME (hrs.) [28,55](2,4)
Mg X
COUNTS(X10¹)
TIME (hrs.) [37,60](2,4)
O VI
COUNTS(X10²)
TIME (hrs.) [28,55](2,4)
O VI
COUNTS(X10²)
TIME (hrs.) [37,60](2,4)

Figure 15

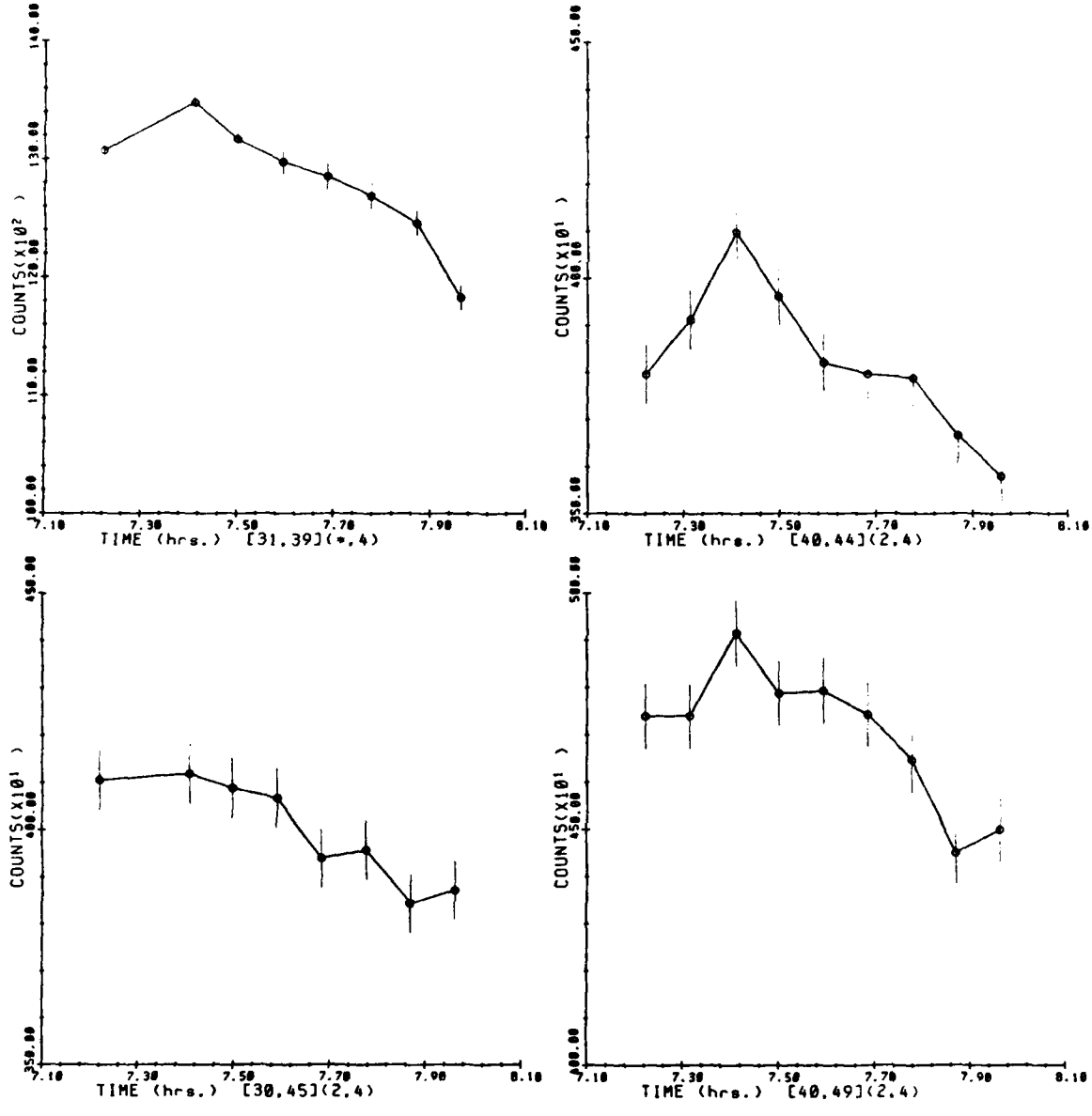
COUNTS(X10²)
TIME (hrs.) [31,39](*,4)
COUNTS(X10¹)
TIME (hrs.) [40,44](2,4)
COUNTS(X10¹)
TIME (hrs.) [30,45](2,4)
COUNTS(X10¹)
TIME (hrs.) [40,49](2,4)

Figure 16

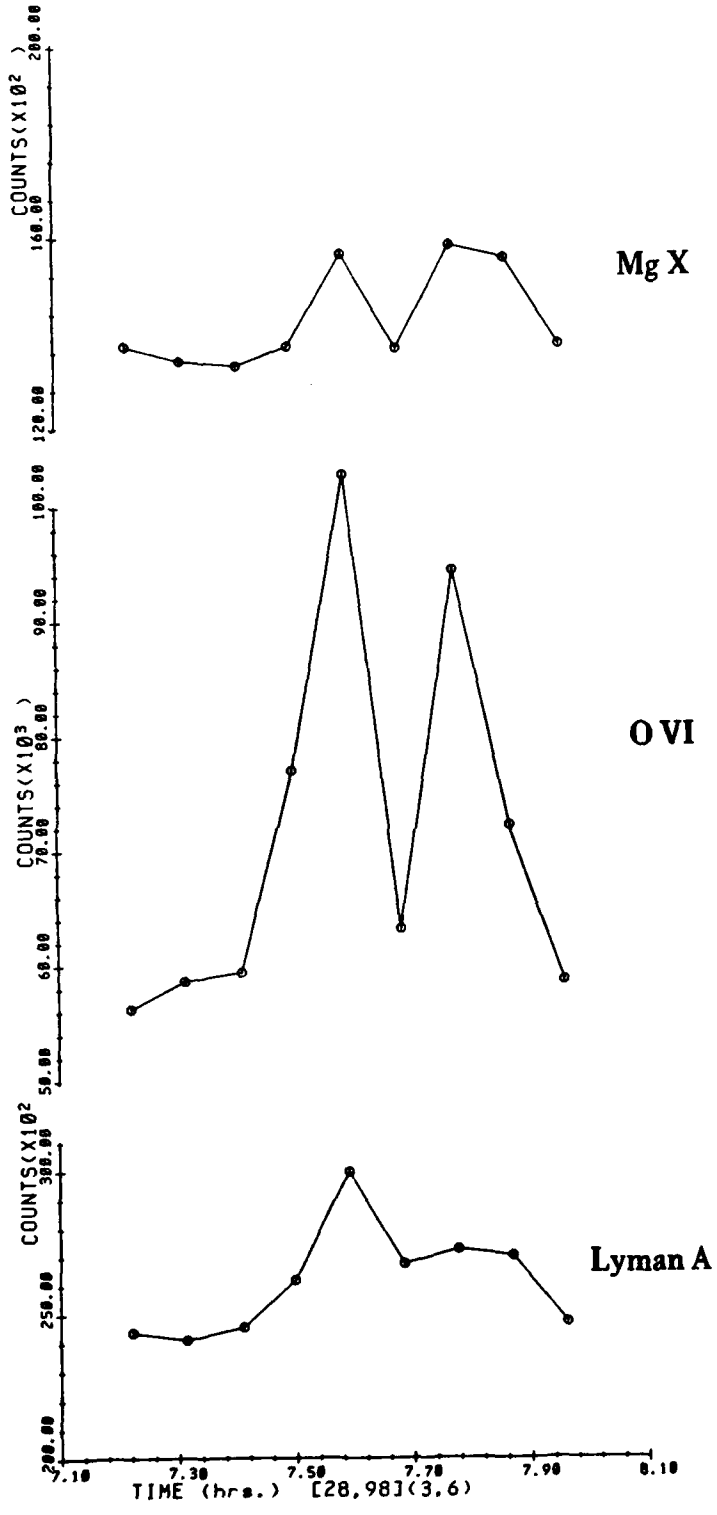
COUNTS(X10²)
200.00
160.00
120.00
Mg X
COUNTS(X10³)
100.00
90.00
80.00
70.00
60.00
50.00
O VI
COUNTS(X10²)
300.00
250.00
200.00
Lyman A
7.10
7.30
7.50
7.70
7.90
8.10
TIME (hrs.) [28,98](3,6)

Figure 17

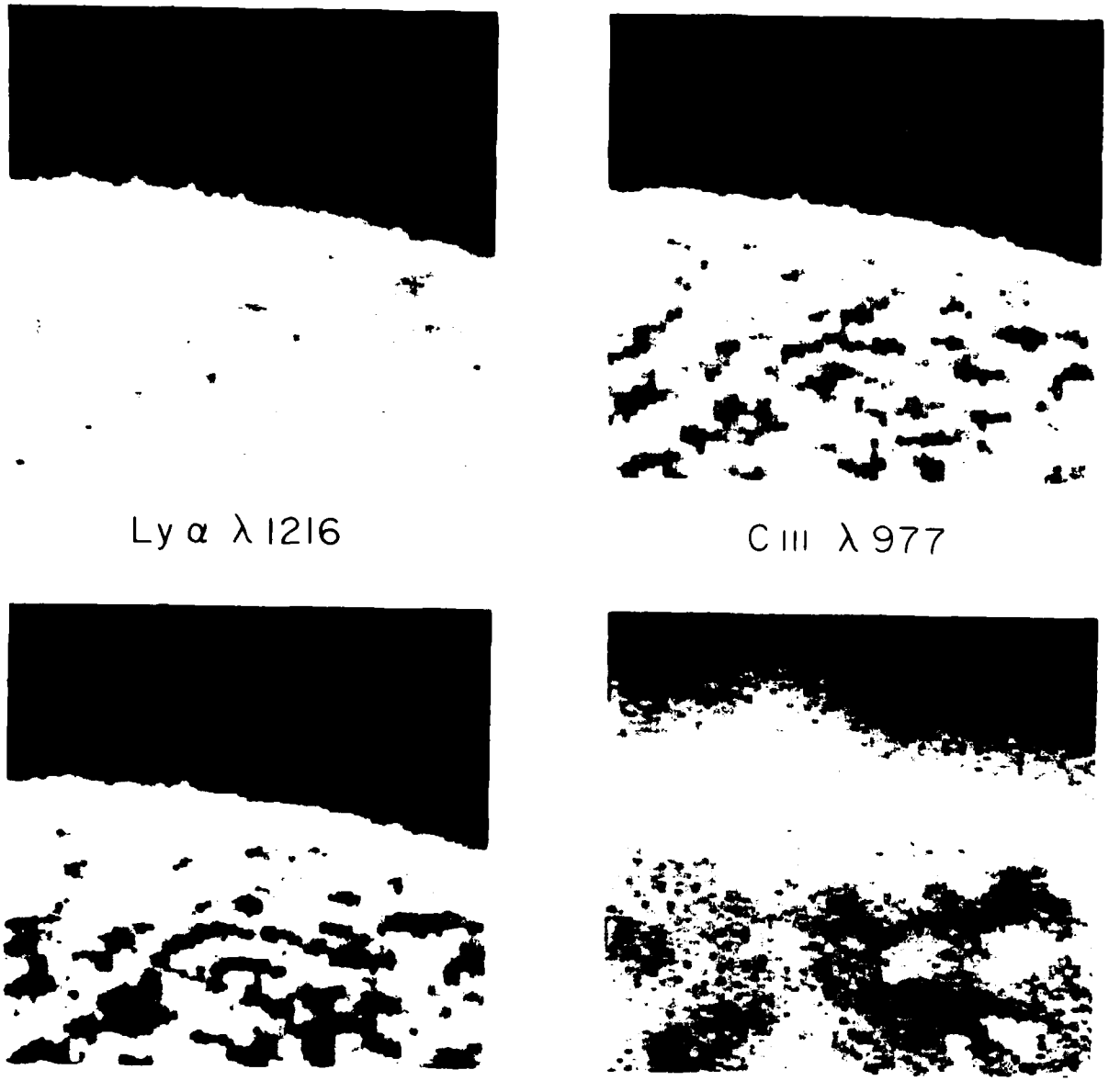
Ly α λ 1216
C III λ 977
O VI λ 1032
Mg X λ 625
QUIET NE LIMB
5 JANUARY 1974

Figure 18

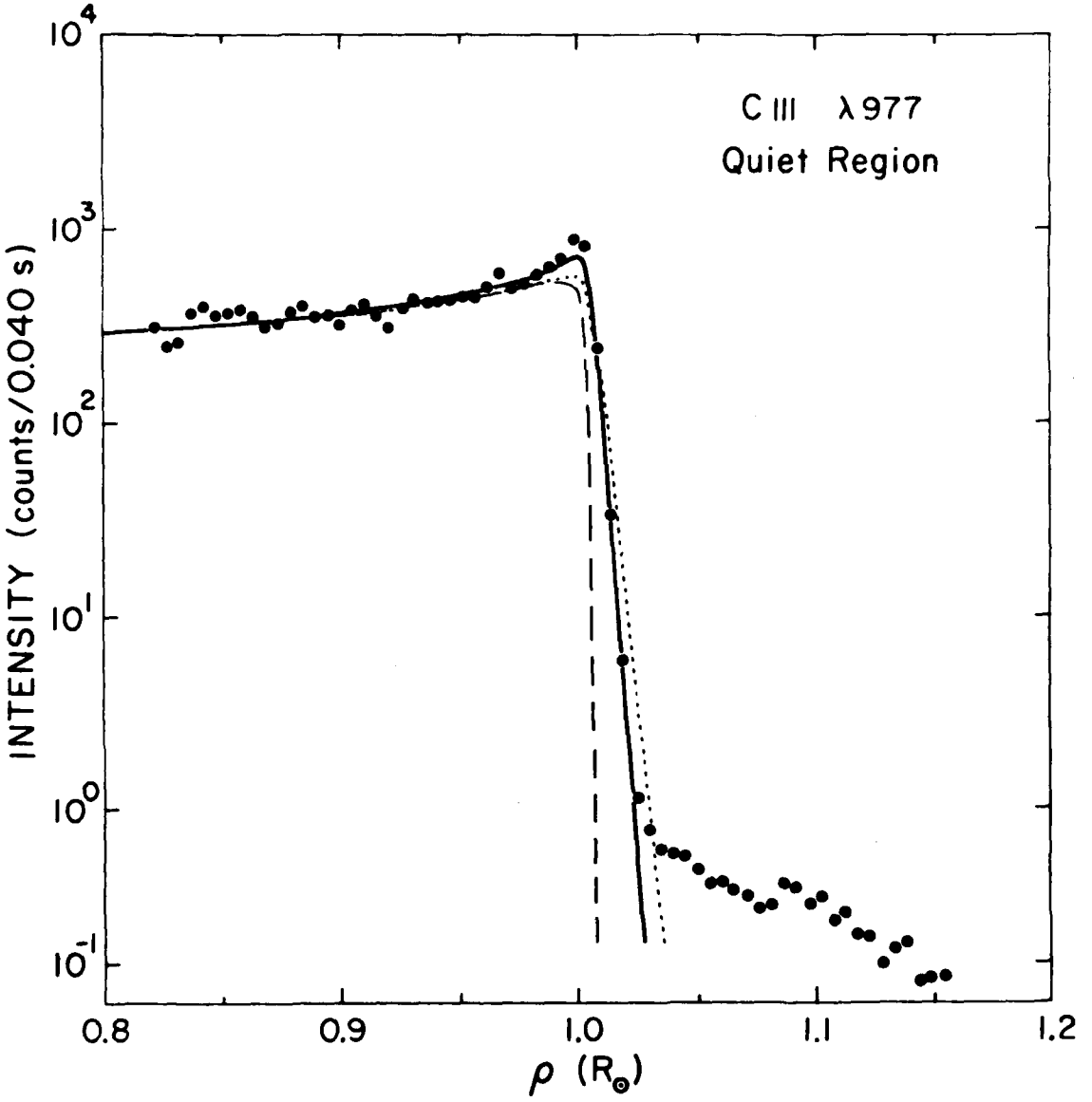
C III λ977
Quiet Region
INTENSITY (counts/0.040 s)
10^4
10^3
10^2
10^1
10^0
10^{-1}
0.8
0.9
1.0
1.1
1.2
ρ (R⊙)

Figure 19

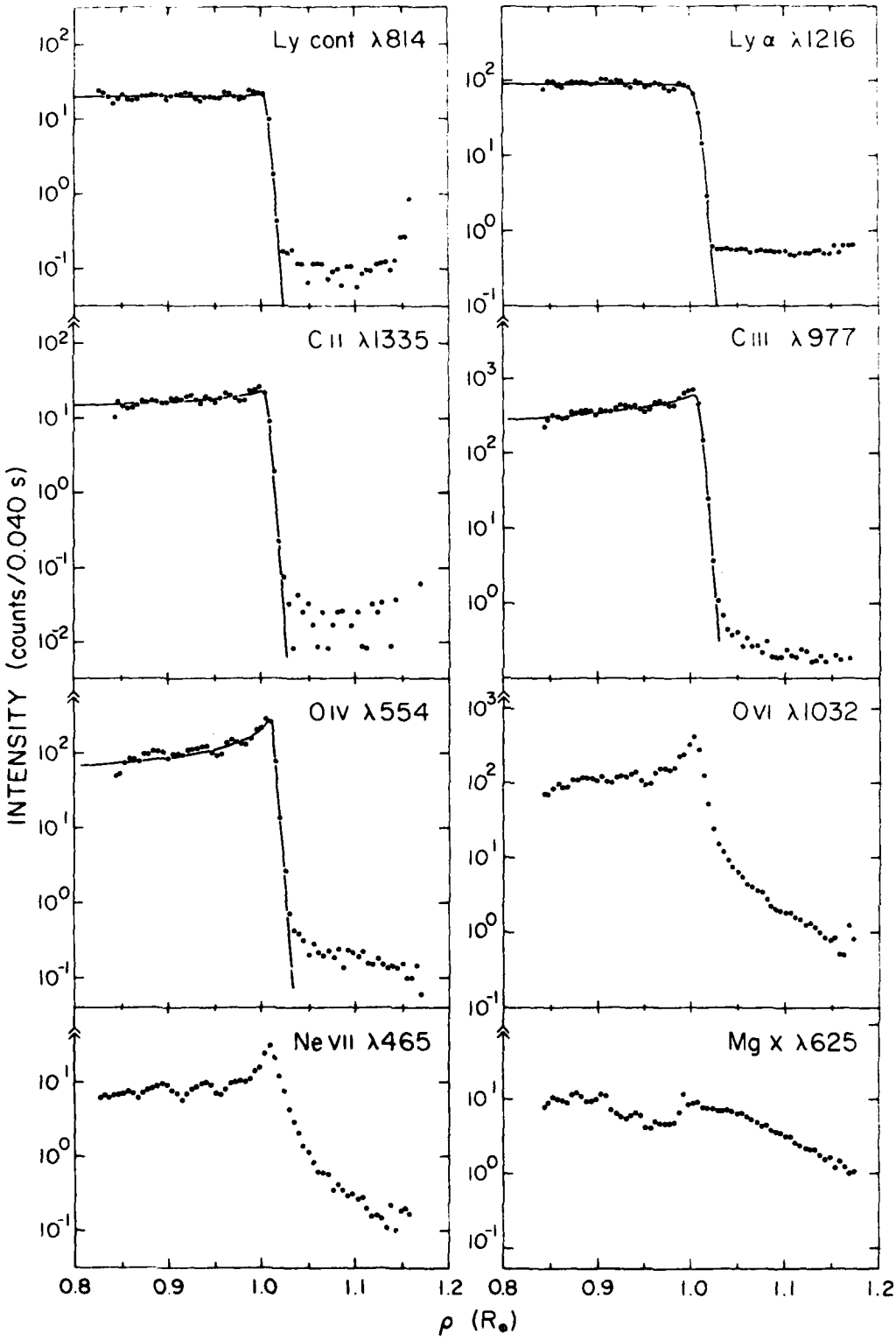
Ly cont λ814
Ly α λ1216
C II λ1335
C III λ977
O IV λ554
O VI λ1032
Ne VII λ465
Mg X λ625
INTENSITY (counts/0.040 s)
ρ (R⊙)
0.8
0.9
1.0
1.1
1.2

Figure 20

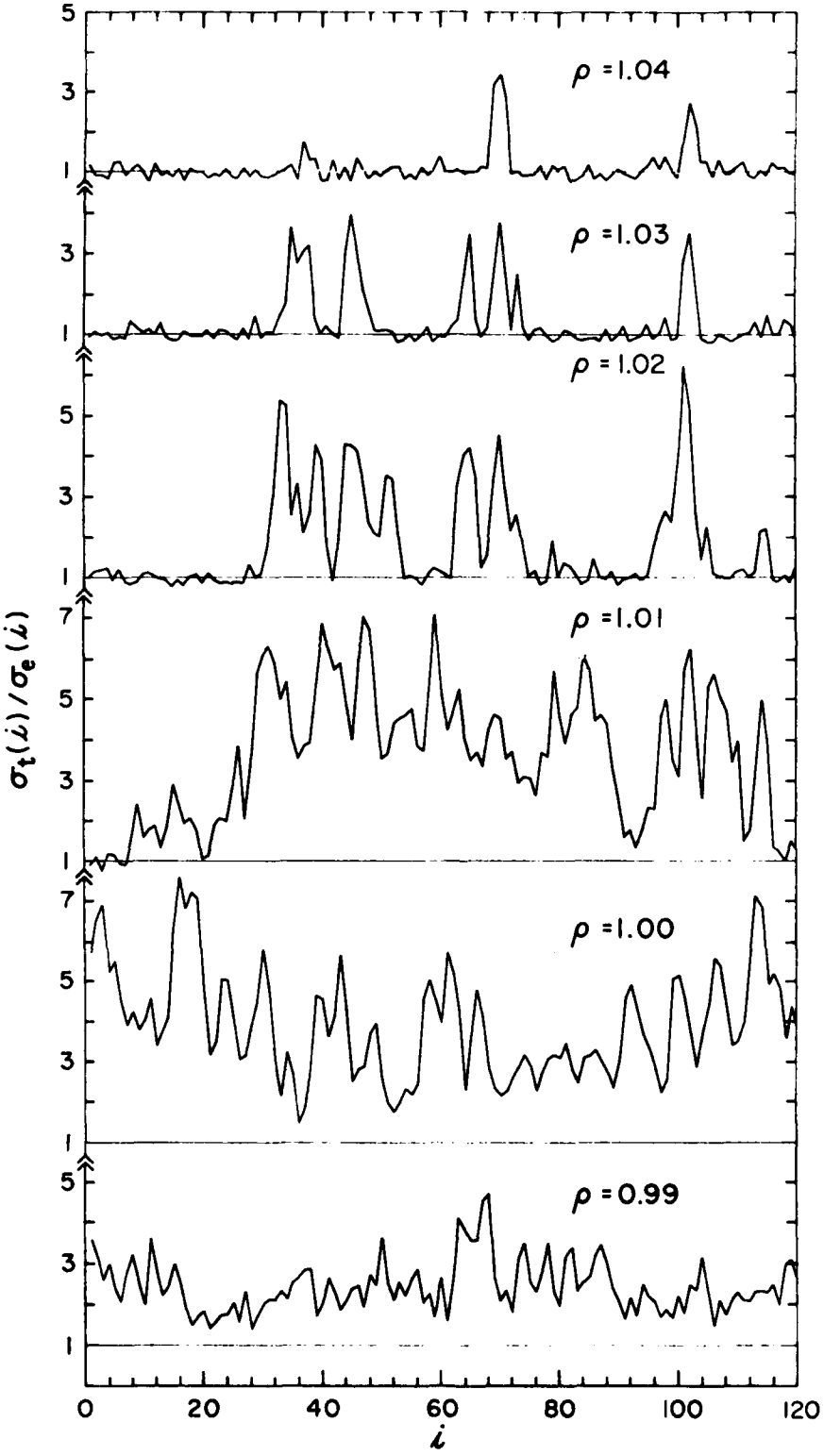

Figure 21

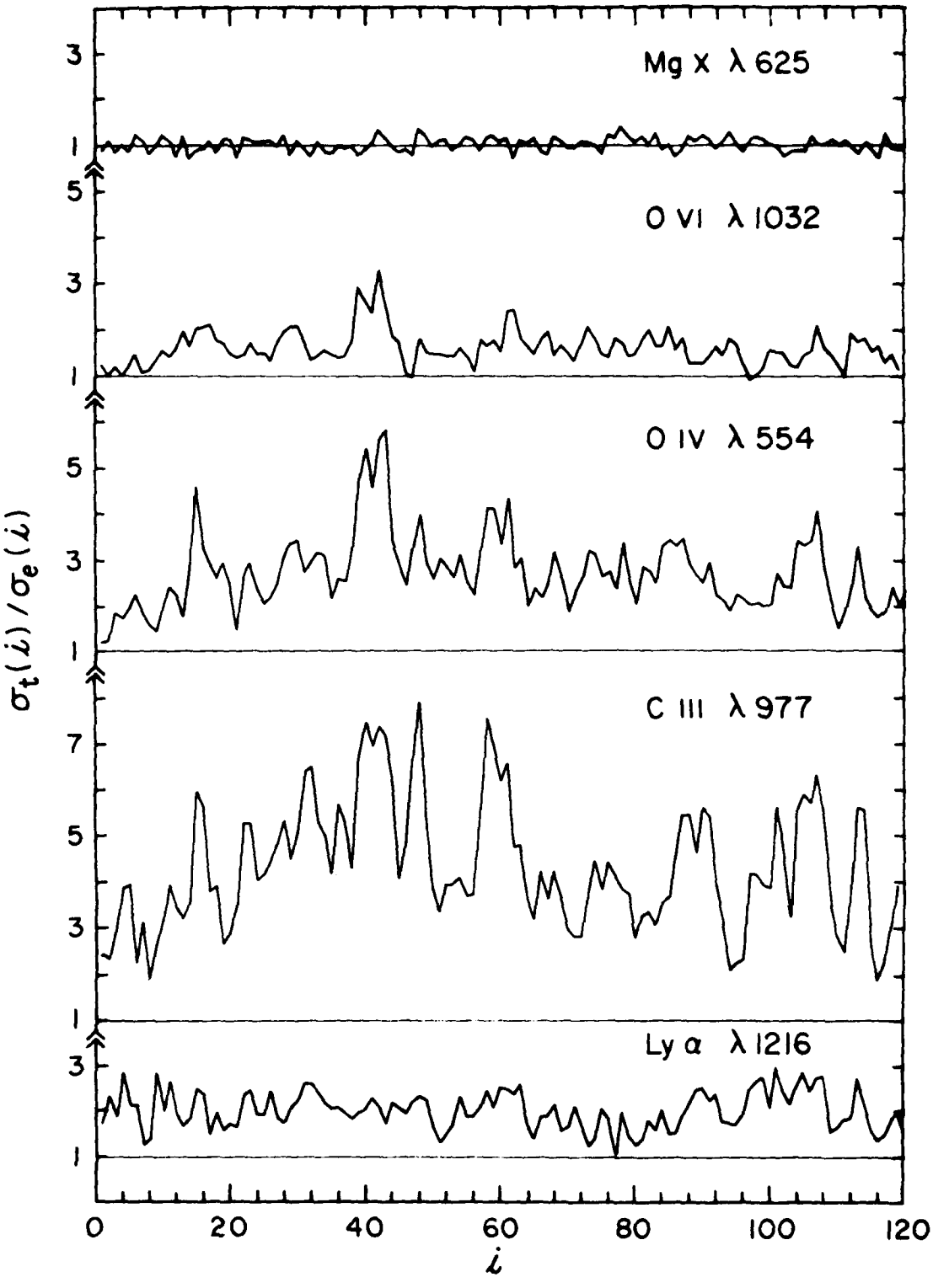
Mg X λ 625
O VI λ 1032
O IV λ 554
C III λ 977
Ly α λ 1216
$\sigma_t(i) / \sigma_e(i)$
i
0
20
40
60
80
100
120

Figure 22

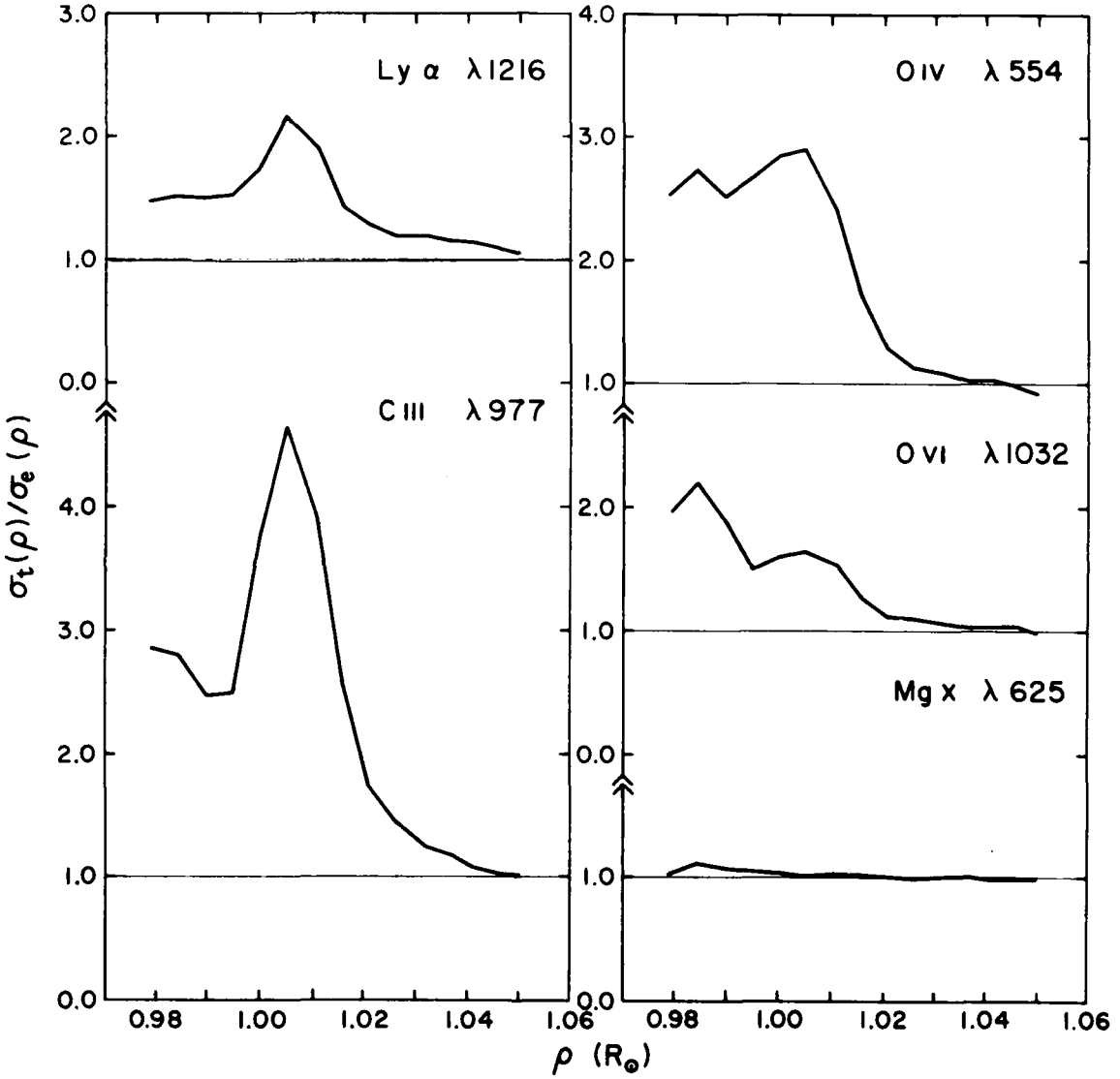
Ly α λ1216
O IV λ 554
C III λ 977
O VI λ 1032
Mg X λ 625
$\sigma_t(\rho)/\sigma_e(\rho)$
ρ ($R_\odot$)
0.98
1.00
1.02
1.04
1.06

Figure 23

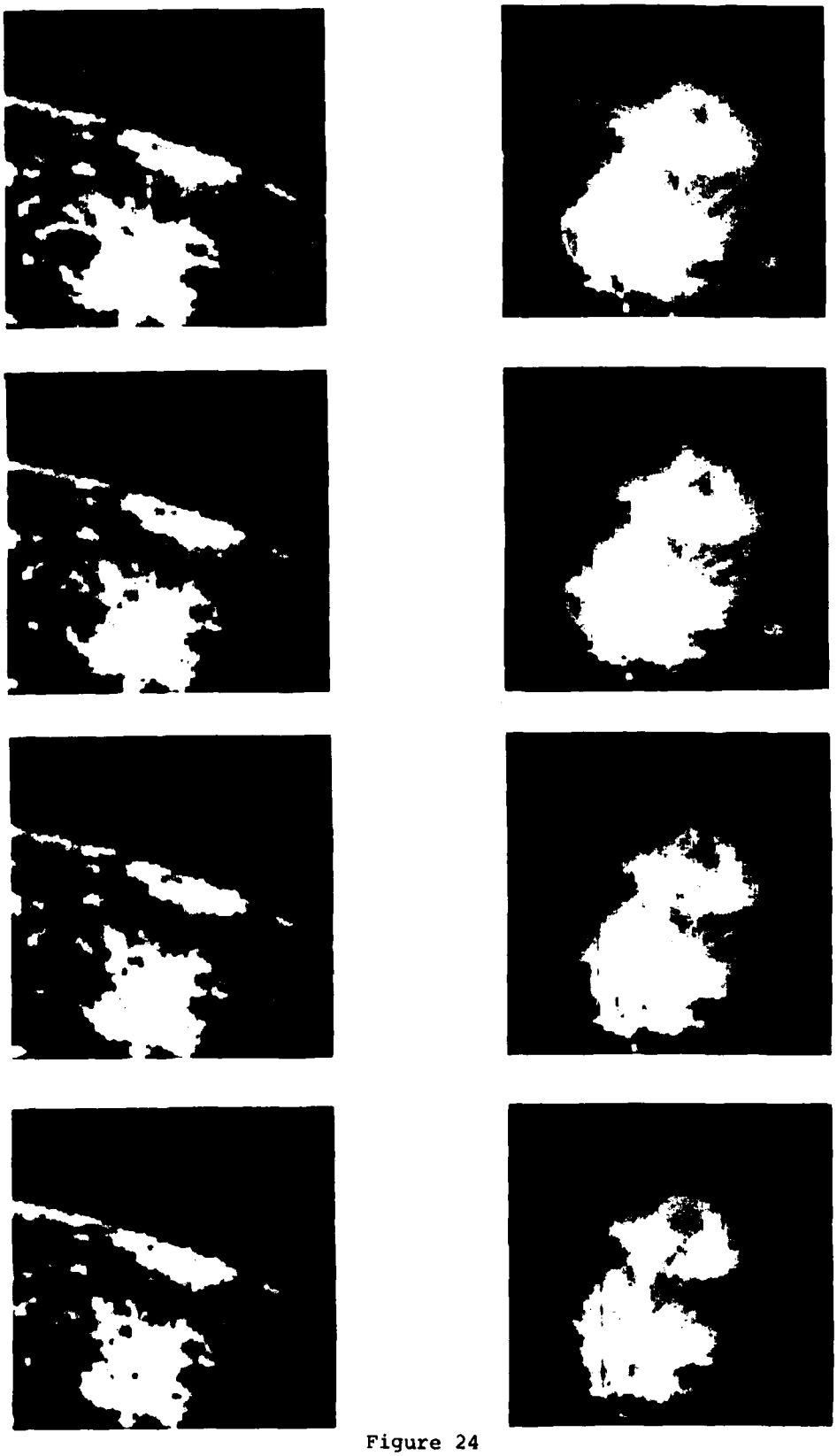

Figure 24

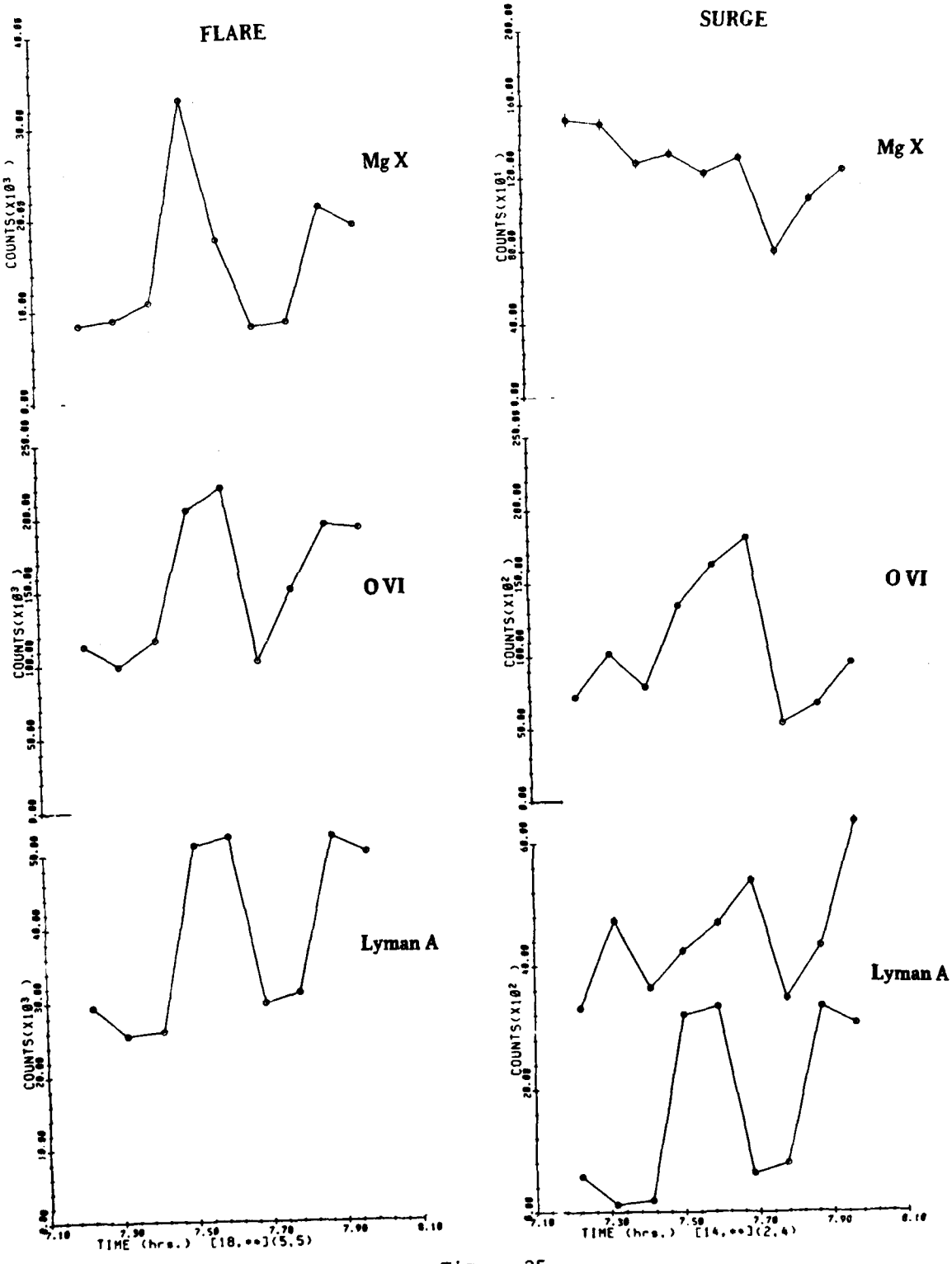
FLARE
SURGE
Mg X
O VI
Lyman A
COUNTS(X10³)
COUNTS(X10²)
COUNTS(X10¹)
TIME (hrs.) [18,**](5,5)
TIME (hrs.) [14,**](2,4)

Figure 25

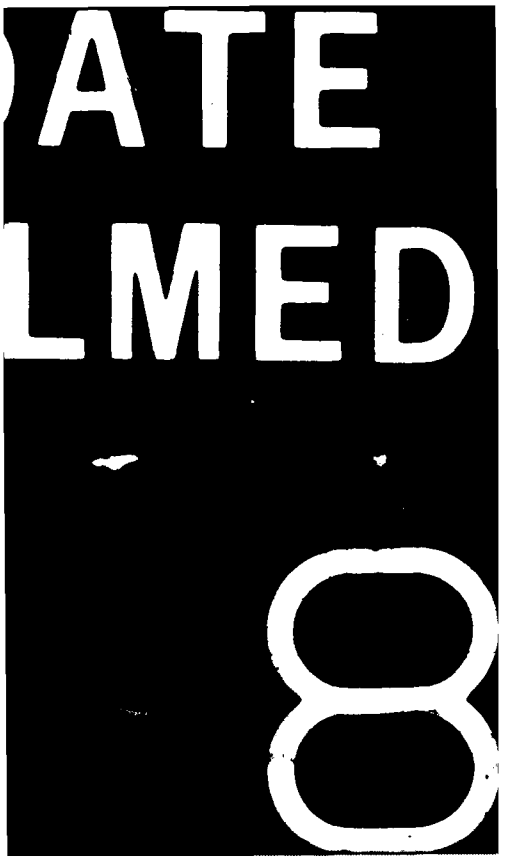
ATE
LMED
8